HHS Public Access

Author manuscript

Kidney Int. Author manuscript; available in PMC 2017 September 05.

Published in final edited form as:

Kidney Int. 2016 June ; 89(6): 1307–1323. doi:10.1016/j.kint.2016.03.006.

Loss of *Glis2/NPHP7* causes kidney epithelial cell senescence and suppresses cyst growth in the Kif3a mouse model of cystic kidney disease

Dongmei Lu[1], **Alysha Rauhauser**[1], **Binghua Li**[1], **Chongyu Ren**[1], **Kayla McEnery**[1], **Jili Zhu**[1,2], **Moumita Chaki**[1], **Komal Vadnagara**[1], **Sarah Elhadi**[3], **Anton M. Jetten**[4], **Peter Igarashi**[5], and **Massimo Attanasio**[1,6]

[1]Department of Internal Medicine, University of Texas Southwestern Medical Center, Dallas, TX, USA

[2]Department of Nephrology, Renmin Hospital, Wuhan University, Wuhan, Hubei, China

[3]Department of Pediatrics, University of Texas Southwestern Medical Center, Dallas, TX, USA

[4]Cell Biology Section, Division of Intramural Research, National Institute of Environmental Health Sciences, National Institutes of Health, Research Triangle Park, NC, USA

[5]Department of Internal Medicine, University of Minnesota, Minneapolis, MN, USA

[6]Eugene McDermott Center for Growth and Development, University of Texas Southwestern Medical Center, Dallas, TX, USA

Abstract

Enlargement of kidney tubules is a common feature of multiple cystic kidney diseases in humans and mice. However, while some of these pathologies are characterized by cyst expansion and organ enlargement, in others, progressive interstitial fibrosis and kidney atrophy prevail. The *Kif3a* knockout mouse is an established non-orthologous mouse model of cystic kidney disease. Conditional inactivation of *Kif3a* in kidney tubular cells results in loss of primary cilia and rapid cyst growth. Conversely, loss of function of the gene *GLIS2/NPHP7* causes progressive kidney atrophy, interstitial inflammatory infiltration, and fibrosis. *Kif3a* null tubular cells have unrestrained proliferation and reduced stabilization of p53 resulting in a loss of cell cycle arrest in the presence of DNA damage. In contrast, loss of *Glis2* is associated with activation of checkpoint kinase 1, stabilization of p53, and induction of cell senescence. Interestingly, the cystic phenotype of *Kif3a* knockout mice is partially rescued by genetic ablation of *Glis2* and pharmacological stabilization of p53. Thus, Kif3a is required for cell cycle regulation and the DNA damage response, whereas cell senescence is significantly enhanced in *Glis2* null cells. Hence, cell senescence is a central feature in nephronophthisis type 7 and Kif3a is unexpectedly required for efficient DNA damage response and cell cycle arrest.

Correspondence: Massimo Attanasio, University of Texas Southwestern Medical Center, 5323 Harry Hines Boulevard, Dallas, TX, 75390, USA. massimo.attanasio@utsouthwestern.edu.

DISCLOSURE

All the authors declared no competing interests.

Supplementary material is linked to the online version of the paper at www.kidney-international.org.

Keywords

cystic kidney disease; DNA damage; Kif3a; nephronophthisis; senescence

The term cystic kidney disease refers to several conditions that have in common cystic expansion of renal tubules. In some cases, such as in polycystic kidney disease, cystic growth is the prevalent feature and is sustained by highly proliferating cells lining multiple fluid-filled cysts originating from tubular segments, a feature that caused this disease to be dubbed “neoplasia in disguise.”[1,2] On the other hand, kidneys in nephronophthisis (NPHP), a group of autosomal recessive cystic diseases, which represent the most frequent genetic cause of renal failure in the first 3 decades of life,[3] are often decreased in volume, due to progressive tubular atrophy and interstitial fibrosis. Virtually, all the proteins encoded by the genes mutated in cystic kidney diseases are localized to the primary cilium of kidney epithelial cells.[4,5] The primary cilium is an important subcellular organelle and its integrity has been shown to be required for the correct functioning of several signaling pathways, including hedgehog (Hh) signaling.[6-9] Interestingly, recent evidence has shown that several ciliary proteins are unexpectedly related to the regulation of cellular response to DNA damage and DNA repair.[10-12] The kinesin Kif3a is among the many proteins necessary for the building of primary cilia, and kidney-specific inactivation of *Kif3a* in mice results in loss of cilia and rapid cyst formation in the kidneys.[13] On the contrary, loss of function of the gene *GLIS2/NPHP7*, a repressor of Hh signaling,[13] causes a NPHP-like phenotype in humans and mice, characterized by progressive kidney atrophy, interstitial inflammatory infiltration, and fibrosis.[5,13,14] This suggests that different mechanisms underlie the kidney phenotype of these 2 mouse models of cystic kidney disease, which possibly affect cell proliferation and apoptosis. The protein Glis2 is a paralog of another Hh inhibitor, Gli3, whose activity is dependent on primary cilia.[9] To investigate a possible dependence of Glis2 on primary cilia and whether additional mechanisms are determining the kidney phenotype in *Glis2* knockouts, we knocked out *Glis2* in a mouse with kidney-specific (Ksp) inactivation of *Kif3a* ($^{\text{Ksp-}cre}Kif3a^{f/-}$). We found that genetic inactivation of *Glis2* in kidney-specific *Kif3a* knockout mice, partially suppresses uncontrolled cell proliferation, cyst growth, and tubular apoptosis in this mouse model of cystic kidney disease. We show that immortalized tubular epithelial cells derived from *Kif3a* null kidneys display impaired stabilization of p53 in the presence of spontaneous DNA damage, defective activation of the G1/S checkpoint, ectopic cyclin B1 expression, and failure to arrest in the cell cycle, with consequent increased rates of cell duplication and apoptosis. Oppositely, stable *Glis2* short hairpin RNA (shRNA)-mediated silencing is accompanied by activation of the serine-threonine-specific checkpoint kinase 1 (Chk1), stabilization of p53, and induction of cell senescence, a permanent cell cycle arrest, which reduces DNA damage and apoptosis in *Kif3a* null cells. Importantly, *in vivo*, pharmacological stabilization of p53, using an inhibitor of the protein mouse double minute 2 (MDM2), partially rescued cyst growth, tubular proliferation, and apoptosis in $^{\text{Ksp-}cre}Kif3a^{f/-}$ mice. Our findings indicate that Kif3a is required for cell cycle regulation and its loss results in impaired DNA damage response, whereas loss of *Glis2* induces abnormal activation of Chk1 and promotes cell senescence. These results indicate that cell senescence is a central feature in NPHP type 7 and reveal an unexpected requirement of Kif3a for efficient DNA damage response and cell cycle arrest.

RESULTS

Glis2 inactivation in Ksp-*cre*$Kif3a^{f/-}$ knockouts results in reduced cyst growth, improved renal function, and decreased tubular cell proliferation and apoptosis

Glis2, a repressor of Hh signaling is localized at the primary cilia of kidney epithelial cells, as its orthologs Gli1, Gli2, and Gli3.[5,13,14,] Intact primary cilia are required for correct functioning of Gli3, another repressor of the Hh signaling pathway.[9] To determine whether Glis2 functions are also dependent on primary cilia, we performed a standard epistasis experiment, by inactivating *Glis2* in kidney-specific $Kif3a^{f/-}$ knockout mice.[15,16] We generated Ksp-*cre*$Kif3a^{f/-}$;$Glis2^{mut/mut}$ double knockout-transgenic mice (indicated in the figures simply as $Kif3a^{f/-}$;$Glis2^{-/-}$ for graphical purposes) from $Glis2^{mut/mut}$ null mice,[14] $Kif3a^{+/f}$,[16] $Kif3a^{+/-}$[17] mice, and the Ksp-*cre* transgenic mouse.[15] Kidneys of Ksp-*cre*$Kif3a^{f/-}$ mice develop severe cystic kidney disease early in life and die at about 6 weeks of age.[16] $Glis2^{mut/mut}$ kidneys, instead, show increased expression of genes related to inflammation and tissue repair at young ages (extracellular matrix proteases, matrix chemokines, and cytokines) but develop tubular atrophy and interstitial fibrosis only later in life.[5,14] We evaluated the morphology of paraffin-embedded kidneys of Ksp-*cre*$Kif3a^{f/-}$;$Glis2^{mut/mut}$ double knockout-transgenic mice at postnatal day P30 and compared it with Ksp-*cre*$Kif3a^{f/-}$;$Glis2^{+/mut}$ mice of the same age (Figure 1a and Supplementary Figure S1). Kidneys of Ksp-*cre*$Kif3a^{f/-}$;$Glis2^{mut/mut}$ double knockouts had delayed cyst growth, as shown by decreased kidney–total body weight ratio, reduced cystic area per total kidney area, and reduced average cyst size (Figure 1b). Ksp-*cre*$Kif3a^{f/-}$;$Glis2^{mut/mut}$ double knockouts also had lower levels of blood urea nitrogen and serum creatinine than Ksp-*cre*$Kif3a^{f/-}$;$Glis2^{+/mut}$ mice did (Figure 1c). To determine whether reduced cyst growth in kidneys of Ksp-*cre*$Kif3a^{f/-}$;$Glis2^{mut/mut}$ double knockouts is associated with decreased cellular proliferation or increased apoptosis, we examined the rates of proliferation of tubular epithelial cells in Ksp-*cre*$Kif3a^{f/-}$;$Glis2^{mut/mut}$ double knockouts and Ksp-*cre*$Kif3a^{f/-}$;$Glis2^{+/mut}$ single mutants. This was accomplished by using antibodies against the cell cycle antigen Ki67 and an antibody against activated caspase 3 (aCasp3) that marks apoptotic cells. The proliferation index, expressed as percentage of Ki67-positive cells over total number of cells per optical field, was the highest in Ksp-*cre*$Kif3a^{f/-}$;$Glis2^{+/mut}$ and significantly reduced in Ksp-*cre*$Kif3a^{f/-}$;$Glis2^{mut/mut}$ double mutants (Figure 1d, upper panels, and e). Similarly, apoptosis in tubular cells was higher in Ksp-*cre*$Kif3a^{f/-}$;$Glis2^{+/mut}$ single mutants and decreased in Ksp-*cre*$Kif3a^{f/-}$;$Glis2^{mut/mut}$ double knockouts (Figure 1d, lower panels, and f). Primary cilia were absent in cysts of both Ksp-*cre*$Kif3a^{f/-}$ and Ksp-*cre*$Kif3a^{f/-}$;- $Glis2^{mut/mut}$ mice (Supplementary Figure S2A). Interestingly, expression of *Gli1*, one of the target genes of Hh that can be used as readout of the activation of this signaling pathway, was increased in Ksp-*cre*$Kif3a^{f/f}$ immortalized cells[8] (Supplementary Figure S2B). We conclude that *Glis2* inactivation reduces kidney cyst growth and preserves renal function in the Kif3a mouse model of polycystic kidney disease by reducing tubular cell proliferation and not by inducing apoptosis.

Kif3a null kidney epithelial cells have accelerated cell cycle

To acquire more details about the causes of the high tubular proliferation rate observed in Ksp-*cre*$Kif3a^{f/-}$ knockout mice *in vivo*, we examined the cell cycle of the previously

described immortalized Ksp-*cre**Kif3a*$^{f/f}$ kidney epithelial cell line[8] (reported shortly as *Kif3a*$^{f/f}$ in the figures for graphical purposes) by flow cytometry and compared it with Ksp-*cre**Kif3a*$^{+/f}$ hemizygous cells as a control. Neither protein expression nor subcellular localization of Glis2 was significantly affected by the absence of *Kif3a* (Supplementary Figure S3A and B). We noticed that a higher proportion of Ksp-*cre**Kif3a*$^{f/f}$ cells than the control cells were in the S and G2/M phases of the cell cycle (Figure 2a and b). Then, we generated stable *Glis2* knockdown cell lines from both Ksp-*cre**Kif3a*$^{f/f}$ null and Ksp-*cre**Kif3a*$^{+/f}$ hemizygous cells by lentivirus-mediated shRNA infection and assessed knock-down efficiency by Western blot (Supplementary Figure S3A). Interestingly, stable inactivation of *Glis2* by shRNA-mediated silencing (indicated as *Glis2*^{KD} in the figures, KD for knock-down) in Ksp-*cre**Kif3a*$^{f/f}$ cells significantly decreased the proportion of cycling cells (Figure 2a and b). The accelerated cell cycle of the immortalized Ksp-*cre**Kif3a*$^{f/f}$ cells was further assessed by measuring cellular proliferation via a tetrazolium dye colorimetric assay (MTT) (Figure 2c) and by demonstrating increased bromodeoxyuridine (BrdU) incorporation (Figure 2d) in null cells compared with Ksp-*cre**Kif3a*$^{+/f}$ heterozygous control cells. Primary tubular cells obtained from Ksp-*cre**Kif3a*$^{f/-}$;*Glis2*$^{mut/mut}$ double knockouts had also higher proportion of cells in G1 and longer doubling time than did Ksp-*cre**Kif3a*$^{f/-}$ single mutant cells (Figure 2e). Although no differences in the cell cycle were noticed between Ksp-*cre**Kif3a*$^{f/-}$ and wild-type cells by flow cytometry cell cycle analysis, due to the overall slower proliferation rates of primary cells compared with the immortalized clones in which a residual activity of the SV40 antigen may still be present, increased proliferation of Ksp-*cre**Kif3a*$^{f/-}$ primary cells was clearly detectable by the MTT assay (Figure 2f). Collectively, these experiments indicate that the higher proliferation rate of *Kif3a* null kidney epithelial cells is cell-autonomous and their cell cycle anomaly is rescued by inactivation of *Glis2*.

Kif3a null kidney epithelial cells exhibit increased DNA damage and apoptosis

High cellular proliferation rates are often associated with increased DNA damage due to genotoxic stress (stalling of replication forks and incomplete DNA replication) and increased production of oxygen radicals, secondary to the alteration of the mitochondrial metabolism.[18] Because of the high proliferation rates exhibited by Ksp-*cre**Kif3a*$^{f/f}$ cells, we tested the occurrence of DNA damage in Ksp-*cre**Kif3a*$^{f/f}$ cells versus Ksp-*cre**Kif3a*$^{+/f}$ control cells, using an antibody against the phosphorylated histone 2AX (γH2AX). Histone 2AX is recruited at sites of DNA breaks, where it is phosphorylated on Ser139 by the protein kinase ataxia-telangiectasia-mutated (ATM),[19] and is commonly used as a marker of DNA damage. [20] Ksp-*cre**Kif3a*$^{f/f}$ cells, compared with the Ksp-*cre**Kif3a*$^{+/f}$ control cells, had significantly increased DNA damage (measured by determining the average number of positive foci per nucleus in immunofluorescence confocal microscopy images) (Figure 3a and b) Similar results were also observed by Western blot (Figure 3c). Furthermore, the number of γH2AX foci in Ksp-*cre**Kif3a*$^{f/f}$ null cells dramatically decreased after shRNA-mediated *Glis2* silencing (Figure 3a). With the exception of Ksp-*cre**Kif3a*$^{+/f}$;*Glis2*$^{KD-5.2}$, which may be related to clonal variability, *Glis2* knock-down, Ksp-*cre**Kif3a*$^{+/f}$ heterozygous cells had more DNA damage than did the nontargeted control, but was lower than Ksp-*cre**Kif3a*$^{f/f}$ knockout cells. Similarly, sections of Ksp-*cre**Kif3a*$^{f/-}$;*Glis2*$^{+/mut}$ kidneys showed higher proportion of cells with DNA damage than did Ksp-*cre**Kif3a*$^{f/+}$;*Glis2*$^{mut/mut}$

mice, and the number of tubular cells positive for γH2AX was significantly reduced in Ksp-*cre*$Kif3a^{f/-}$;$Glis2^{mut/mut}$ double mutants (Figure 3b, e, and f). Collectively, these results suggest that both *Kif3a* and *Glis2* null cells are subject to DNA damage, which is higher in *Kif3a* knockout cells than in *Glis2* null cells. However, concomitant inactivation of *Glis2* is associated with reduced DNA damage in *Kif3a* knockout cells.

Ksp-*cre*$Kif3a^{f/f}$ kidney epithelial cells have defective G1/S cell cycle checkpoint in the presence of DNA damage

The coexistence of diffuse DNA damage and accelerated cell cycle in Ksp-*cre*$Kif3a^{f/f}$ null cells was surprising, because diffuse DNA damage is expected to activate DNA damage response and cell cycle arrest, in order to allow DNA repair and avoid the transmission of compromised genetic material to daughter cells.[21] In the presence of DNA damage, the DNA damage response blocks the cell cycle at the transition between the G1 and S phase (G1/S checkpoint), preventing initiation of replication. There is also a block between prophase and anaphase, before the onset of mitosis (G2/M checkpoint), that impedes progression through mitosis. We tested the competency of the G1/S and the G2/M checkpoints in the Ksp-*cre*$Kif3a^{f/f}$ null cell line: cells were synchronized in G1 using double block with thymidine to prevent them from entering the S phase, or in G2 with nocodazole, which interferes with the organization of the spindle microtubules in prophase and prometaphase and prevents cells to undergo mitosis. To assess the state of the G1/S checkpoint, we measured by flow cytometry the fraction of G1-synchronized Ksp-*cre*$Kif3a^{f/f}$ and Ksp-*cre*$Kif3a^{+/f}$ cells that transit into the S phase of the cell cycle after thymidine washout. After release of the thymidine block (Figure 4a and b), the percentage of Ksp-*cre*$Kif3a^{f/f}$ cells progressing into the S phase was higher than for the heterozygous control cells, indicating a decreased competency of the G1/S restriction point, which was restored after shRNA-mediated silencing of *Glis2*. The ratio of cells in G2/M 6 hours after release of prolonged nocodazole block was lower in Ksp-*cre*$Kif3a^{f/f}$ cells than in Ksp-*cre*$Kif3a^{+/f}$ control cells and was increased after shRNA-mediated *Glis2* silencing, suggesting a possible activation of the G2/M checkpoint (Figure 4c and Supplementary Figure S4). Because this experiment only identifies cells with 4n DNA content, but does not distinguish between premitotic (G2) and mitotic (M) cells, we performed bivariate flow cytometry analysis, using an antibody against phosphorylated histone H3 (pHis3), a nuclear antigen present only in mitotic cells.[11,22] The fraction of cells in mitosis was about one-half in Ksp-*cre*$Kif3a^{f/f}$ null cells compared with Ksp-*cre*$Kif3a^{+/}$ control cells (Figure 4d to f and Supplementary Figure S5). These results indicate that the G1/S checkpoint is defective in Ksp-*cre*$Kif3a^{f/f}$ null cells and it is rescued by concomitant inactivation of *Glis2*. The G2/M checkpoint, in contrast, is effective in Ksp-*cre*$Kif3a^{f/f}$ null cells, suggesting that the increased proportion of cells transiting through the G2/M phase after *Glis2* shRNA silencing reported in Figure 4c is a secondary effect due to reduction of DNA damage.

Kif3a and *Glis2* null kidney epithelial cells have defective and excessive activation of p53, respectively

The presence of numerous nuclear γH2AX foci in Ksp-*cre*$Kif3a^{f/f}$ cells indicated that detection of DNA damage and activation of the early stages of the DNA repair cascade are not compromised, suggesting that downstream mechanisms are implicated in the lack of

G1/S competency in these cells. In mammals, DNA damage is principally sensed by the protein kinases, ATM, ataxia telangiectasia, and Rad3-related (ATR), which propagate the signal through the phosphorylation of 2 downstream kinases, Chk1 and Chk2. To explore the state of these kinases, we examined levels of Chk1 and Chk2 and their activated phosphorylated forms (Ser345 of Chk1, Ser19 of Chk2) in Ksp-*cre*$Kif3a^{f/f}$ and Ksp-*cre*$Kif3a^{+/f}$ cells, with and without concomitant *Glis2* silencing, by Western blot. We observed more Chk2 activation in Ksp-*cre*$Kif3a^{f/f}$ cells than in Ksp-*cre*$Kif3a^{+/f}$ control cells, independent of *Glis2* silencing in all the tested cell lines (Figure 5a, upper panels). In contrast, no differences in Chk1 phosphorylation were evident between Ksp-*cre*$Kif3a^{f/f}$ and Ksp-*cre*$Kif3a^{+/f}$, but this kinase was strongly activated in both cell lines after shRNAmediated silencing of *Glis2*, suggesting that the normalizing effect of $Glis2^{KD}$ on Ksp-*cre*$Kif3a^{f/f}$ cells' cycle may be associated with the activation of Chk1 (Figure 5a, middle panels). Chk2 and Chk1 are nonrelated kinases with partially overlapping functions that phosphorylate common substrates to promote cell cycle arrest.[23] The tumor suppressor p53 is one of the principal effectors downstream of Chk1 and Chk2, and it is phosphorylated and stabilized by these 2 kinases.[19,23,24] By Western blot, we found that compared with Ksp-*cre*$Kif3a^{+/f}$ heterozygous control cells, Ksp-*cre*$Kif3a^{f/f}$ cells have slightly higher content of p53 that increased after *Glis2* silencing (Figure 5a, lower panels). To verify whether this pattern occurred *in vivo*, we first examined by immunofluorescence microscopy sections of Ksp-*cre*$Kif3a^{f/-}$;$Glis2^{+/mut}$ kidneys, using an antibody against p53 and noticed that numerous interstitial cells were positive for p53 (Figure 5b). For this reason, in order to test the status of p53 exclusively in tubular epithelial cells, we obtained primary tubular cell cultures from kidneys of Ksp-*cre*$Kif3a^{f/-}$;$Glis2^{+/mut}$, Ksp-*cre*$Kif3a^{f/-}$;$Glis2^{mut/mut}$, $Glis2^{mut/mut}$, and wild-type mice and assayed their p53 content by Western blot. p53 was undetectable in wild-type and Ksp-*cre*$Kif3a^{f/-}$;$Glis2^{+/mut}$ lysates, but it was increased in Ksp-*cre*$Kif3a^{f/-}$;$Glis2^{mut/mut}$, $Glis2^{mut/mut}$ mice (Figure 5c, upper panels). In the same way, the ratio of activated Chk1 to total Chk1 was low in Ksp-*cre*$Kif3a^{f/-}$ primary cells, increased in $Glis2^{mut/mut}$ cells, and highest in Ksp-*cre*$Kif3a^{f/-}$;$Glis2^{mut/mut}$ (Figure 5c, lower panels). These results indicate that *Kif3a* and *Glis2* null kidney epithelial cells have defective and excessive activation of Chk1 and p53, respectively, and suggest that the decreased proliferation in Ksp-*cre*$Kif3a^{f/-}$;$Glis2^{mut/mut}$ double mutants compared with Ksp-*cre*$Kif3a^{f/-}$;$Glis2^{+/mut}$ mice is related to activation of p53.

Kif3 null kidney epithelial cells present ectopic accumulation of cyclin B1 and genomic instability

An important effect of p53 activation on the cell cycle is mediated by repressing the transcription and stability of cyclin B1.[25,26] The cellular concentration of cyclin B1 increases during the G2 phase of the cell cycle and abruptly falls after its ubiquitination by anaphase promoting complex (APC) at the onset of mitosis. We determined the levels of cyclin B1 by flow cytometry using a specific fluorescein isothiocyanate-conjugated antibody against cyclin B1 in Ksp-*cre*$Kif3a^{f/f}$ and Ksp-*cre*$Kif3a^{+/f}$ cells, with or without concomitant *Glis2* shRNA-mediated silencing. Cyclin B1 expression was higher in Ksp-*cre*$Kif3a^{f/f}$ cells than in heterozygous control cells and was reduced in both cell lines after shRNA-mediated inactivation of *Glis2* (Figure 6a and b and Supplementary Figure S6). In addition, we noticed that the distribution of cyclin B1 content along the cell cycle was also abnormal,

being present not only in G2 but also in S and late G1 phases (Figure 6a, upper left panel, and Supplementary Figure S6), suggesting the possibility of premature mitosis in Ksp-*cre*$Kif3a^{f/f}$ cells. To test this hypothesis, we probed Ksp-*cre*$Kif3a^{f/f}$ cells and Ksp-*cre*$Kif3a^{+/f}$ control cells with an antibody against the phosphorylated threonine 187 of $p27^{Kip1}$ ($^{T187}p27^{Kip1}$). T187 phosphorylation of $p27^{Kip1}$ occurs only in late G1, when it triggers $p27^{Kip1}$ ubiquitination, allowing cells to exit G1 and progress into the S phase of the cell cycle, and it is thus a marker of early phases of the cell cycle.[27] Since $^{T187}p27^{Kip1}$ is only found in late G1 phase and not in premitotic cells, we tested whether metaphase Ksp-*cre*$Kif3a^{f/f}$ and Ksp-*cre*$Kif3a^{+/f}$ cells, recognized by the presence of condensed chromosomes, were positive for $^{T187}p27^{Kip1}$ (Figure 6c). Seven of 7 Ksp-*cre*$Kif3a^{f/f}$ mitotic cells and 1 of 12 Ksp-*cre*$Kif3a^{+/f}$ hemizygous cells were positive for $^{T187}p27^{Kip1}$ ($P < 0.001$ by χ-square statistics, $n = 3$ slides), indicating that Ksp-*cre*$Kif3a^{f/f}$ cells have an uncoordinated cell cycle that leads to anticipated chromosome condensation and mitosis in the presence of still uncompleted DNA duplication. Such a cell cycle defect is consistent with the reduced DNA amount of the Ksp-*cre*$Kif3a^{f/f}$ cells in G2/M (Figure 4a) and it is expected to be associated with centrosome aberrations and polyploidy. In fact, we frequently detected polyploidy by flow cytometry (Figure 6d) by immunofluorescence confocal microscopy in Ksp-*cre*$Kif3a^{f/f}$ but not in Ksp-*cre*$Kif3a^{+/f}$ immortalized epithelial cells (Figure 6e). This was also associated with centrosomal fragmentation (86% of Ksp-*cre*$Kif3a^{f/f}$ and 4% Ksp-*cre*$Kif3a^{+/f}$, $P < 0.0001$ by χ-square statistics, $n = 3$ slides), as previously reported for *Kif3a* null fibroblasts[28] (Figure 6e). Finally, we also observed polyploid cells and megakarya by bright field microscopy in hematoxylin and eosin–stained kidney sections of Ksp-*cre*$Kif3a^{f/-}$ mice, but not in Ksp-*cre*$Kif3a^{f/-}$;$Glis2^{mut/mut}$ double knockouts ($n = 3$ mice) (Figure 6f). These results suggest that the cell cycle abnormality in the absence of *Kif3a* results in repeated DNA endoreduplication, DNA damage, and apoptosis in Ksp-*cre*$Kif3a^{f/-}$ kidneys, and that *Glis2* silencing-dependent activation of p53 limits these defects.

Pharmacological stabilization of p53 reduces cyst growth in Ksp-*cre*$Kif3a^{f/-}$ kidneys

To further substantiate the role of p53 stabilization in partially reducing cyst growth in the Ksp-*cre*$Kif3a^{f/-}$;$Glis2^{mut/mut}$ double mutants, we treated 10- to 12-day-old Ksp-*cre*$Kif3a^{f/-}$ mice with the small-molecule nutlin-3, an inhibitor of MDM2,[29] at the dose of 40 μg/g on alternated days for 10 days.[30] MDM2 is an E3 ubiquitin protein ligase and is a major inducer of p53 degradation.[31] Compared with vehicle-treated control mice of the same age, nutlin-3 treatment resulted in decreased kidney–total body weight ratio, cyst area over total kidney area, average cyst size, and improved renal function (Figure 7a and b and Supplementary Figure S7). Similar to what was observed in Ksp-*cre*$Kif3a^{f/-}$;$Glis2^{mut/mut}$ double mutants, kidneys of nutlin-3-treated mice also showed reduction of proliferation and apoptosis of tubular cells (Figure 7c and d). These results indicate that stabilization of p53 is sufficient to slow cystic progression and prevent cell proliferation and apoptosis in *Kif3a* null kidneys.

Loss of *Glis2* induces cell senescence in kidney epithelial cells

Cell cycle arrest after p53 stabilization allows cells to repair damaged DNA. In cases of irreparable damage, cells may either undergo apoptosis or, alternatively, permanently exit the cell cycle and become senescent. Senescence can be mediated by p53 and is actuated

through epigenetic silencing of genes implicated in cell proliferation, and results in condensed nuclear areas called senescence-associated heterochromatin foci.[32-34] To test for signs of senescence in Ksp-*cre*$Kif3a^{f/f}$ immortalized kidney epithelial cells, we quantified the number of senescence-associated heterochromatin foci using an antibody against tri-methylated lysine 9 of histone 3 (H3K9me3), a marker of heterochromatin found in senescent cells.[35] Ksp-*cre*$Kif3a^{f/f}$ cells had significantly less foci than the hemizygous Ksp-*cre*$Kif3a^{+/f}$ control cells, whereas the number of foci was significantly increased in both Ksp-*cre*$Kif3a^{f/f}$ and Ksp-*cre*$Kif3a^{+/f}$ cells after stable shRNA-mediated silencing of *Glis2* (Figure 8a and b). Western blots also showed increased amount of H3K9me3 in lysates of both Ksp-*cre*$Kif3a^{f/f}$ and Ksp-*cre*$Kif3a^{+/f}$ cells after *Glis2* silencing, but not in cells infected with nontargeting shRNA (Figure 8c). *In vivo*, we found more H3K9me3-positive cells in kidneys of Ksp-*cre*$Kif3a^{f/-}$;$Glis2^{mut/mut}$ mice than in Ksp-*cre*$Kif3a^{f/-}$;$Glis2^{+/mut}$ mice (Figure 8d and e), suggesting that genetic inactivation of *Glis2* induces cell cycle arrest by triggering cellular senescence in Ksp-*cre*$Kif3a^{f/-}$ knockout kidneys. To further test this possibility, we detected the activity of the senescence-associated lysosomal β-galactosidase, a marker that is widely used to identify senescent cells,[36] on fresh kidney sections. Concordant with H3K9me3 content, senescence-associated lysosomal β-galactosidase activity was virtually absent in Ksp-*cre*$Kif3a^{f/-}$;$Glis2^{+/mut}$ kidneys but was clearly detected in Ksp-*cre*$Kif3a^{f/-}$;$Glis2^{mut/mut}$ double mutants and more intensely in $Glis2^{mut/mut}$ kidneys (Figure 8f). Finally, p16, another marker of senescent cells, was upregulated both at RNA and protein level in primary cultures of proximal tubular cells of $Glis2^{mut/mut}$ knockouts and of Ksp-*cre*$Kif3a^{f/-}$;$Glis2^{mut/mut}$ double mutants but not in Ksp-*cre*$Kif3a^{f/-}$;$Glis2^{+/mut}$ and wild-type kidneys (Figure 8g and h and Supplementary Figure S8). Collectively, these results indicate that genetic inactivation of *Glis2* induces senescence in both wild-type and *Kif3a* null kidney tubular cells.

DISCUSSION

Tubule dilation and cyst formation, accompanied by a certain degree of tubular cell proliferation and apoptosis, are characteristics shared by most, if not all, cystic kidney diseases, including NPHP and polycystic kidney disease. Nonetheless, although pronounced cyst growth is prevalent in some forms of cystic kidney disease, such as polycystic kidney disease, progressive organ atrophy and fibrosis are typical features of NPHP. In this study we have examined the Ksp-*cre*$Kif3a^{f/-}$ kidney-specific knockout mouse, in which kidneys are characterized by rapid cyst growth, and the $Glis2^{mut/mut}$ mouse model of NPHP type 7, which reproduces virtually all the features of human NPHP, including diffuse tubular atrophy, interstitial inflammatory infiltration, fibrosis, and progressive decrease in kidney size.[5,14,16] The data that we have presented indicate that 2 opposite molecular mechanisms underlie the phenotype in these 2 mouse models of cystic kidney disease. On one side, we unexpectedly found that the kinesin *Kif3a* is required for regulation of the cell cycle, activation of Chk1, stabilization of p53, and cell cycle arrest, which are all compromised in its absence. Loss of *Glis2*, on the other hand, induces sustained Chk1 activation, execution of the DNA damage response and cell senescence, which is the principal cause of the NPHP phenotype in the *Glis2* knockout mouse. The exact mechanism by which senescence is evoked in *Glis2* null cells is still unclear, but the abnormal activation of Chk1 that we have

observed, is suggestive that replicative stress during the S phase of the cell cycle may be the primary cause of senescence in these cells.[37] Interestingly, other ciliary proteins associated with ciliopathy phenotypes have recently been shown to be required for correct activation and functioning of the pathways that control the cellular response to DNA damage,[10-12,38-41] suggesting that permanent cell cycle arrest and senescence could be a common feature of these diseases. In this regard, it is worth noticing that expression of many secreted factors (extracellular matrix proteases, matrix components, chemokines, and cytokines), recognized as part of the senescence secretory–associated phenotype[42] are upregulated in *Glis2* null kidneys.[5,14] This correlation provides a possible explanation of the progressive kidney interstitial inflammation typical of NPHP. Irrespective of the upstream mechanisms of Chk1 activation, it is very likely that the consequent stabilization of p53 is central in determining the actuation of senescence in *Glis2* null cells. The strong Chk1 activation and p53 stabilization in the absence of *Glis2* is also likely to drive the partial rescue of the *Kif3a* knockout mice cystic phenotype. Our experiments suggest that the absence of *Kif3a* extensively perturbs the cell cycle, with consequent genomic instability and DNA damage, but at the same time results in defective activation of Chk1 and DNA repair. Loss of *Glis2*, instead, by inducing Chk1-mediated DNA damage response, stabilizes p53 with consequent decreased proliferation and DNA damage in the *Kif3a* null cells. This model would account for the apparent paradox that loss of *Glis2* increases DNA damage in *Kif3a* hemizygous cells but has opposite effects in *Kif3a* null cells that have higher levels of DNA damage. Less clear is why loss of *Glis2* does not seem to significantly affect the cell cycle of *Kif3a* hemizygous immortalized tubular cells, at least *in vitro*. One possibility is that the coexistence of other mechanisms, such as the epithelial-to-mesenchymal transition that is characteristic of the *Glis2* knockout cells,[5,13] may prevail on the cell cycle arrest in *Kif3a* hemizygous cells. Another question that will need to be addressed is whether the unrestrained cell cycle and the defective activation of Chk1 in *Kif3a* null cells is consequent to loss of cilia or centrosome-related functions of this kinesin, considering that cilia have been widely related to the cell cycle and many of the proteins that regulate DNA damage response (such as several cyclins and cyclindependent kinases, p53, Chk1, and Chk2) are found in the centrosomes.[43-45] Understanding this point may help to better define the relationship between the ciliary dependent procystogenic signal that is activated in the absence of polycystins and the one that acts in the *Kif3a* knockouts and is dependent on loss of primary cilia.[46] It is interesting, in any case, that anomalies of DNA damage and repair, defective activation of p53, and genomic instability seem to be common to multiple cystic kidney diseases, including autosomal dominant polycystic kidney disease, pointing to an association between hyperproliferation and cell cycle dysregulation in these diseases.[47-49] In conclusion, we have shown that *Kif3a* null cells have an accelerated cell cycle, impaired stabilization of p53, and an inability to trigger DNA damage response–dependent cell cycle arrest. Contrarily, loss of *Glis2* results in excessive activation of Chk1 and cell senescence, which is a central feature in NPHP type 7 and one that partially rescues the hyperproliferation of *Kif3* defective cells and the cystic phenotype of *Kif3a* knockout kidneys.

MATERIALS AND METHODS

Animal studies

Ksp-*cre*$Kif^{f/-}$ mice express Cre recombinase in kidney epithelial cells and were previously described.[16] The phenotypes of Ksp-*cre*$Kif^{f/-}$;$Glis2^{+/mut}$ and Ksp-*cre*$Kif^{f/-}$;$Glis2^{+/mut}$ mice were compared with those of Ksp-*cre*$Kif^{f/-}$;$Glis2^{mut/mut}$ double knockouts and Ksp-*cre*$Kif^{f/+}$;$Glis2^{mut/mut}$ mice. For pharmacological stabilization of p53, the small molecule nutlin-3 was diluted in dimethylsulfoxide and injected intraperitoneally on alternate days for 2 weeks starting from P10 to P12 at the dose of 40 μg/g. All animal studies were approved by the Institutional Animal Care and Use Committees from the University of Texas Southwestern Medical Center.

Blood urea nitrogen and serum creatinine

Blood samples were obtained by periorbital capillary puncture. Creatinine concentrations were measured using a P/ACE MDQ Capillary Electrophoresis System (Beckman Coulter, Brea, CA) at 214 nm.[50] Blood urea nitrogen measurements were obtained using the Vitros 250 chemistry analyzer (GMI Inc., Ramsey, MN).

Digital image analysis

Whole kidneys stained with hematoxylin and eosin were imaged using Zeiss Axioscan Z1 microscope (Jena, Germany). Quantification of cyst number and cyst area were obtained by digital elaboration of microscope images using the ImageJ software (National Institutes of Health, Bethesda, MD; http://rsb.info.nih.gov/ij/).

Cell cultures

$Kif3a^{f/f}$ and $Kif3a^{f/+}$ cells obtained by SV40 T-mediated immortalization as previously described[8] were grown at permissive temperature (33 °C) in the presence of 0.1 unit/ml interferon-γ and allowed to differentiate at 37 °C without interferon for at least 3 days before the experiment.

Primary tubular cell cultures

Primary tubular cells were isolated from kidneys of experimental mice (21–30 days old) after digestion of cortex fragments with collagenase and cultured under sterile conditions, according to a previously described method.[51] After 7 days, cell cultures formed a confluent monolayer and were used for the experiments.

Glis2 silencing by lentiviral shRNA-mediated vector cell infection

Glis2-targeting shRNA vectors packed for lentiviral infection were used to create stable cell clones as previously described.[13] Clones were named based on the targeting shRNA used (for example, $Kif3a^{f/f}$;$Glis2^{KD\text{-}5.1}$ corresponds to clone 1 obtained by infecting $Kif3a^{f/f}$ with the shRNA construct 5; $Kif3a^{f/f}$;$Glis2^{KD\text{-}7.2}$ corresponds to clone 2 obtained by infecting $Kif3a^{f/f}$ with the shRNA construct 7; and so on). Clones were chosen based on the efficiency of the shRNA constructs.

Antibodies

Beta actin (A3854), alpha-tubulin (T6074), gamma-tubulin (SAB503045), and antiacetylated α-tubulin (6-11B-1) were purchased from Sigma (St. Louis, MO). Cleaved caspase-3 (AB3623MI) was from Fisher Scientific (Thermo Fisher Scientific, Waltham, MA). Ser139 phospho-histone H2A (9178) Chk1 (2360), Chk2 (2662) Ser345 phospho-Chk1 (2348), Ser19 phpspho-Chk2 (2666), and Ser10 pHis3 fluorescently conjugated pHis3 (9708) were from Cell Signaling (Danvers, MA). Ki67 (ab15580), p53 (ab26), H3K9Me3 (ab8898), and p16 (51243) were from Abcam (Cambridge, MA). Kip1 (phospho Thr187) antibody was from GeneTex (Irvine, CA). Anti-Aurora kinase B was purchased from BD Biosciences (611082; San Jose, CA), and the Glis2 polyclonal antibody was described previously.[13]

MTT proliferation assay

Life technologies stock solution was prepared using sterile phosphate-buffered saline (PBS; 5 mg MTT/ml). Cells were seeded in 96-well plates and allowed to attach for 24 hours and fresh medium was supplemented with 100 μl of MTT (3-[4,5-dimethylthiazol-2-yl]-2,5-diphenyltetrazolium bromide) was added to each well. Cells were then incubated in the dark at 37 °C for 2 hours, medium with MTT was removed, and 100 μl of dimethylsulfoxide per well was added to stop the reaction. Absorbance was read at λ = 540 nM using an automatic plate reader.

Senescence-associated β-galactosidase staining

Fresh PBS perfused unfixed kidneys were obtained from experimental mice. Samples were placed in optimal cutting temperature compound on top of dry ice. Then, 10-μm cryosections were washed in PBS, fixed in 4% formaldehyde, and then incubated at 37 °C for 12 to 16 hours with fresh 5-bromo-4-chloro-3-indolyl β-D-galactosidase (X-Gal, 1 mg of per ml) solution (20 mg of dimethylformamide per ml, 40 mM citric acid/sodium phosphate pH 6.0, 5 mM potassium ferrocyanide, 5 mM potassium ferricyanide, 150 mM $NaCl_2$ mM $MgCl_2$).

Immunofluorescence

Tissues were collected after perfusion with PBS and 4% paraformaldehyde, then fixed in 4% paraformaldehyde for 2 hours on ice, left in a solution of 30% sucrose in PBS at 4 °C overnight, and embedded in optimal cutting temperature compound. Tissue sections were incubated in a solution of 0.1% sodium borohydride ($NaBH_4$) for 30 minutes and incubated in blocking solution (10% goat serum, 0.1% bovine serum albumin [BSA] in PBS) for 1 hour at room temperature. Tissues were incubated overnight at 4 °C with primary antibody diluted in blocking solution and with fluorescently labeled secondary antibody for 1 hour at room temperature. Samples were mounted with ProLong (Life Technologies, Thermo Fisher Scientific) with 4′,6-diamidino-2-phenylindole. Images were acquired using a Zeiss Axioplan 2 deconvolution microscope or a Zeiss LSM 510 confocal microscope with constant acquisition parameters between samples and control cells.

Flow cytometry

Cell cycle analysis—Immortalized cells were allowed to differentiate for 3 days in the absence of γ-interferon at 37 °C, then they were replated and harvested at 50% confluence and fixed with 70% cold ethanol and stained with propidium iodide solution (50 μg/ml, Sigma). Cell cycle distribution was obtained by flow cytometry using a FACS Calibur dual-laser instrument (BD Biosciences). The software FlowJo (FlowJo, Ashland, OR) was used for the data analysis.

Double thymidine block—Cells were synchronized in the G1 phase of the cell cycle by adding thymidine (2.5 mM) to the culture medium for 16 hours in the absence of γ-interferon at 37 °C, allowed to grow in thymidine-free medium for 12 hours, and reexposed to thymidine for an additional 16 hours. An aliquot of cells (time 0) was fixed and used to record synchronization by flow cytometry. The remaining cells were allowed to grow and were harvested at 3, 6, and 8 hours in thymidine-free medium. Cells' DNA was then stained by propidium iodide and the fraction of cells that progressed to the S phase was evaluated by flow cytometry analysis. The numbers here correspond to the ratio between the percentage of cells in G1 after thymidine washout at 3, 6, and 8 hours over the number of cells in G1 before washouts (time 0), multiplied by 100 ($\mathrm{G1}ex.=\frac{\mathrm{G1}.t0-\mathrm{G1}.t\mathrm{n}}{\mathrm{G1}.t0}\bullet 100$).

Nocodazole block—Cells were first synchronized in the G1 phase by adding thymidine (2.5 mM) to the culture medium for 16 hours and grown in thymidine-free medium for 8 hours; then they were synchronized in late G2 phase by growing them in the presence of nocodazole (100 ng/ml) for 20 hours. After this time, all cells were collected, an aliquot was used as a control for achieved synchronization and the remaining cells were washed in PBS and grown in fresh medium without nocodazole for 6 hours. Cells' DNA was then stained by propidium iodide and analysis for DNA content was performed by flow cytometry. The percentage of G2 exiting cells was expressed by cell numbers in G2 at 6 hours divided by the cell numbers in G2 at time 0.[52]

Cumulative BrdU incorporation assay—Cells were seeded at 37 °C in the absence of γ-interferon at low density and allowed to grow for 16 hours. BrdU (10 μg/ml, Sigma) was added to a final concentration of 20 μg/ml. Cells were harvested at 2, 4, and 6 hours; fixed in 4% paraformaldehyde; and incubated with anti-BrdU fluorescently labeled antibody (Abcam) and propidium iodide. BrdU incorporation was determined by flow cytometry, data analysis was performed using the software FlowJo.

Cyclin B1 analysis—Immortalized cells were allowed to differentiate for 3 days in the absence of γ-interferon at 37 °C, then they were replated and harvested at 50% confluence and fixed with 70% cold ethanol. Cells were permeabilized in 0.25% Triton X-100 in PBS, and then resuspended in 100 μl of staining buffer (1% BSA in PBS) containing 0.5 μg of fluorescein isothiocyanate–conjugated cyclin B1 antibody (554108; BD Pharmingen, San Diego, CA) or isotype antibody for 1 hour at room temperature, followed by propidium iodide staining.

pHis3 expression bivariate analysis—Immortalized cells were allowed to differentiate for 3 days in the absence of γ-interferon at 37 °C, and then they were replated and treated with nocodazole (50 ng/ml) for 6 hours. After fixation with ice-cold 70% ethanol, cells were permeabilized with 0.25% Triton X-100/PBS for 15 minutes on ice, blocked with 2% BSA/PBS for 15 minutes, and incubated with anti-pHis3 antibody for 2 hours. Cells were then washed 3 times in PBS and stained with propidium iodide (50 μg/ml, Sigma). Cell cycle distribution was obtained by flow cytometry using a FACS Calibur dual-laser instrument (BD Biosciences). FlowJo software was used for the data analysis.

Quantitative real-time PCR

Total RNA was isolated using TRIzol (Invitrogen, Thermo Fisher Scientific) and purified with Qiagen RNeasy Mini Kit (Alameda, CA). First-strand reverse transcription reactions were performed on 1 μg of total RNA using the ThermoScript RT-PCR Kit (Invitrogen). Real-time polymerase chain reactions (PCRs) were performed using iQ SYBR Green Supermix (Bio-Rad, Berkeley, CA). The following real-time PCR primers were used: p16-Fw CGTACCCCGATTCAGGTGAT; p16-Rev:TTGAGCAGAAGAGCTGCTACGT; betaactin Fw: GGCTGTATTCCCCTCCATCG; beta-actin Rev CCAGTTGGTAACAATGCCATGT. All real-time PCR experiments were performed in triplicates.

Sodium dodecylsulfate–polyacrylamide gel electrophoresis/Western blotting

Protein lysates were mixed with 4× Laemmli sample buffer (161- 0737; Bio-Rad) containing 100 mm dithiothreitol and denatured at 95 °C for 10 minutes. Samples were run on polyacrylamide gels and transferred to polyvinylidene difluoride membranes (LC2002, Thermo Fisher Scientific, Florence, KY). Membranes were blocked in 5% BSA, probed with primary antibody in 1% BSA for 2 hours at room temperature or overnight at 4 °C and with secondary antibody in 1% BSA for 1 hour at room temperature. Antibody binding was visualized with luminol reagent (sc-2048; Santa Cruz Biotechnology, Santa Cruz, CA). When necessary, blots were stripped with 0.1 m tris–hydrochloride, pH 7.8; 10% sodium dodecylsulfate; and 0.70% β-mercaptoethanol for 20 to 30 minutes at 50 °C before reprobing.

Supplementary Material

Refer to Web version on PubMed Central for supplementary material.

Acknowledgments

We would like to thank Patricia Cobo-Stark and Jessica Lucas for their technical support and Dr. Denise Marciano for editing the manuscript. MA was supported by the National Institutes of Health grants (1R01DK090326-01A1, P30DK079328-04), the American Society of Nephrology Norman Siegel award, and the Satellite Healthcare Norman Coplon extramural research award.

References

1. Grantham JJ. Polycystic kidney disease: neoplasia in disguise. Am J Kidney Dis. 1990; 15:110–116. [PubMed: 2405652]

2. Harris PC, Watson ML. Autosomal dominant polycystic kidney disease: neoplasia in disguise? Nephrol Dial Transplant. 1997; 12:1089–1090. [PubMed: 9198029]
3. Hildebrandt F, Attanasio M, Otto E. Nephronophthisis: disease mechanisms of a ciliopathy. J Am Soc Nephrol. 2009; 20:23–35. [PubMed: 19118152]
4. Yoder BK, Hou X, Guay-Woodford LM. The polycystic kidney disease proteins, polycystin-1, polycystin-2, polaris, and cystin, are co-localized in renal cilia. J Am Soc Nephrol. 2002; 13:2508–2516. [PubMed: 12239239]
5. Attanasio M, Uhlenhaut NH, Sousa VH, et al. Loss of GLIS2 causes nephronophthisis in humans and mice by increased apoptosis and fibrosis. Nat Genet. 2007; 39:1018–1024. [PubMed: 17618285]
6. Simons M, Gloy J, Ganner A, et al. Inversin, the gene product mutated in nephronophthisis type II, functions as a molecular switch between Wnt signaling pathways. Nat Genet. 2005; 37:537–543. [PubMed: 15852005]
7. Corbit KC, Shyer AE, Dowdle WE, et al. Kif3a constrains beta-catenin-dependent Wnt signalling through dual ciliary and non-ciliary mechanisms. Nat Cell Biol. 2008; 10:70–76. [PubMed: 18084282]
8. Choi YH, Suzuki A, Hajarnis S, et al. Polycystin-2 and phosphodiesterase 4C are components of a ciliary A-kinase anchoring protein complex that is disrupted in cystic kidney diseases. Proc Natl Acad Sci U S A. 2011; 108:10679–10684. [PubMed: 21670265]
9. Huangfu D, Liu A, Rakeman AS, et al. Hedgehog signalling in the mouse requires intraflagellar transport proteins. Nature. 2003; 426:83–87. [PubMed: 14603322]
10. Chaki M, Airik R, Ghosh AK, et al. Exome capture reveals ZNF423 and CEP164 mutations, linking renal ciliopathies to DNA damage response signaling. Cell. 2012; 150:533–548. [PubMed: 22863007]
11. Choi HJ, Lin JR, Vannier JB, et al. NEK8 links the ATR-regulated replication stress response and S phase CDK activity to renal ciliopathies. Mol Cell. 2013; 51:423–439. [PubMed: 23973373]
12. Airik R, Slaats GG, Guo Z, et al. Renal-retinal ciliopathy gene Sdccag8 regulates DNA damage response signaling. J Am Soc Nephrol. 2014; 25:2573–2583. [PubMed: 24722439]
13. Li B, Rauhauser AA, Dai J, et al. Increased hedgehog signaling in postnatal kidney results in aberrant activation of nephron developmental programs. Hum Mol Genet. 2011; 20:4155–4166. [PubMed: 21816948]
14. Kim YS, Kang HS, Herbert R, et al. Kruppel-like zinc finger protein Glis2 is essential for the maintenance of normal renal functions. Mol Cell Biol. 2008; 28:2358–2367. [PubMed: 18227149]
15. Igarashi P, Shashikant CS, Thomson RB, et al. Ksp-cadherin gene promoter directs kidney-specific expression in transgenic mice. J Am Soc Nephrol. 1998; 9:363A. [PubMed: 9513898]
16. Lin F, Hiesberger T, Cordes K, et al. Kidney-specific inactivation of the KIF3A subunit of kinesin-II inhibits renal ciliogenesis and produces polycystic kidney disease. Proc Natl Acad Sci U S A. 2003; 100:5286–5291. [PubMed: 12672950]
17. Takeda S, Yonekawa Y, Tanaka Y, et al. Left-right asymmetry and kinesin superfamily protein KIF3A: new insights in determination of laterality and mesoderm induction by kif3A$^{-/-}$ mice analysis. J Cell Biol. 1999; 145:825–836. [PubMed: 10330409]
18. Zeman MK, Cimprich KA. Causes and consequences of replication stress. Nat Cell Biol. 2014; 16:2–9. [PubMed: 24366029]
19. Abraham RT. Cell cycle checkpoint signaling through the ATM and ATR kinases. Genes Dev. 2001; 15:2177–2196. [PubMed: 11544175]
20. Sharma A, Singh K, Almasan A. Histone H2AX phosphorylation: a marker for DNA damage. Methods Mol Biol. 2012; 920:613–626. [PubMed: 22941631]
21. Zhou BB, Elledge SJ. The DNA damage response: putting checkpoints in perspective. Nature. 2000; 408:433–439. [PubMed: 11100718]
22. Taylor WR. FACS-based detection of phosphorylated histone H3 for the quantitation of mitotic cells. Methods Mol Biol. 2004; 281:293–299. [PubMed: 15220538]
23. Sancar A, Lindsey-Boltz LA, Unsal-Kacmaz K, Linn S. Molecular mechanisms of mammalian DNA repair and the DNA damage checkpoints. Annu Rev Biochem. 2004; 73:39–85. [PubMed: 15189136]

24. Branzei D, Foiani M. Regulation of DNA repair throughout the cell cycle. Nat Rev Mol Cell Biol. 2008; 9:297–308. [PubMed: 18285803]
25. Innocente SA, Abrahamson JL, Cogswell JP, Lee JM. p53 regulates a G2 checkpoint through cyclin B1. Proc Natl Acad Sci U S A. 1999; 96:2147–2152. [PubMed: 10051609]
26. Nakayama Y, Yamaguchi N. Role of cyclin B1 levels in DNA damage and DNA damage-induced senescence. Int Rev Cell Mol Biol. 2013; 305:303–337. [PubMed: 23890385]
27. Sheaff RJ, Groudine M, Gordon M, et al. Cyclin E-CDK2 is a regulator of p27Kip1. Genes Dev. 1997; 11:1464–1478. [PubMed: 9192873]
28. Kodani A, Salome Sirerol-Piquer M, Seol A, et al. Kif3a interacts with Dynactin subunit p150 Glued to organize centriole subdistal appendages. EMBO J. 2013; 32:597–607. [PubMed: 23386061]
29. Vassilev LT, Vu BT, Graves B, et al. In vivo activation of the p53 pathway by small-molecule antagonists of MDM2. Science. 2004; 303:844–848. [PubMed: 14704432]
30. Endo S, Yamato K, Hirai S, et al. Potent in vitro and in vivo antitumor effects of MDM2 inhibitor nutlin-3 in gastric cancer cells. Cancer Sci. 2011; 102:605–613. [PubMed: 21205074]
31. Ashcroft M, Vousden KH. Regulation of p53 stability. Oncogene. 1999; 18:7637–7643. [PubMed: 10618703]
32. Campisi J, d'Adda di Fagagna F. Cellular senescence: when bad things happen to good cells. Nat Rev Mol Cell Biol. 2007; 8:729–740. [PubMed: 17667954]
33. Campisi J. Cellular senescence: putting the paradoxes in perspective. Curr Opin Genet Dev. 2011; 21:107–112. [PubMed: 21093253]
34. Kuilman T, Michaloglou C, Mooi WJ, Peeper DS. The essence of senescence. Genes Dev. 2010; 24:2463–2479. [PubMed: 21078816]
35. Narita M, Nunez S, Heard E, et al. Rb-mediated heterochromatin formation and silencing of E2F target genes during cellular senescence. Cell. 2003; 113:703–716. [PubMed: 12809602]
36. Dimri GP, Lee X, Basile G, et al. A biomarker that identifies senescent human cells in culture and in aging skin in vivo. Proc Natl Acad Sci U S A. 1995; 92:9363–9367. [PubMed: 7568133]
37. Bartek J, Lukas C, Lukas J. Checking on DNA damage in S phase. Nat Rev Mol Cell Biol. 2004; 5:792–804. [PubMed: 15459660]
38. Otto EA, Hurd TW, Airik R, et al. Candidate exome capture identifies mutation of SDCCAG8 as the cause of a retinal-renal ciliopathy. Nat Genet. 2010; 42:840–850. [PubMed: 20835237]
39. Zhou W, Otto EA, Cluckey A, et al. FAN1 mutations cause karyomegalic interstitial nephritis, linking chronic kidney failure to defective DNA damage repair. Nat Genet. 2012; 44:910–915. [PubMed: 22772369]
40. Slaats GG, Ghosh AK, Falke LL, et al. Nephronophthisis-associated CEP164 regulates cell cycle progression, apoptosis and epithelial-to-mesenchymal transition. PLoS Genet. 2014; 10:e1004594. [PubMed: 25340510]
41. Slaats GG, Saldivar JC, Bacal J, et al. DNA replication stress underlies renal phenotypes in CEP290-associated Joubert syndrome. J Clin Invest. 2015; 125:3657–3666. [PubMed: 26301811]
42. Tchkonia T, Zhu Y, van Deursen J, et al. Cellular senescence and the senescent secretory phenotype: therapeutic opportunities. J Clin Invest. 2013; 123:966–972. [PubMed: 23454759]
43. Plotnikova OV, Pugacheva EN, Golemis EA. Primary cilia and the cell cycle. Methods Cell Biol. 2009; 94:137–160. [PubMed: 20362089]
44. Zhou J. Polycystins and primary cilia: primers for cell cycle progression. Annu Rev Physiol. 2009; 71:83–113. [PubMed: 19572811]
45. Zhang S, Hemmerich P, Grosse F. Centrosomal localization of DNA damage checkpoint proteins. J Cell Biochem. 2007; 101:451–465. [PubMed: 17171639]
46. Ma M, Tian X, Igarashi P, et al. Loss of cilia suppresses cyst growth in genetic models of autosomal dominant polycystic kidney disease. Nat Genet. 2013; 45:1004–1012. [PubMed: 23892607]
47. Nishio S, Hatano M, Nagata M, et al. Pkd1 regulates immortalized proliferation of renal tubular epithelial cells through p53 induction and JNK activation. J Clin Invest. 2005; 115:910–918. [PubMed: 15761494]

48. Battini L, Macip S, Fedorova E, et al. Loss of polycystin-1 causes centrosome amplification and genomic instability. Hum Mol Genet. 2008; 17:2819–2833. [PubMed: 18566106]
49. Burtey S, Riera M, Ribe E, et al. Centrosome overduplication and mitotic instability in PKD2 transgenic lines. Cell Biol Int. 2008; 32:1193–1198. [PubMed: 18725310]
50. Zinellu A, Caria MA, Tavera C, et al. Plasma creatinine and creatine quantification by capillary electrophoresis diode array detector. Anal Biochem. 2005; 342:186–193. [PubMed: 15927140]
51. Terryn S, Jouret F, Vandenabeele F, et al. A primary culture of mouse proximal tubular cells, established on collagen-coated membranes. Am J Physiol Renal Physiol. 2007; 293:F476–F485. [PubMed: 17475898]
52. Whitfield ML, Sherlock G, Saldanha AJ, et al. Identification of genes periodically expressed in the human cell cycle and their expression in tumors. Mol Biol Cell. 2002; 13:1977–2000. [PubMed: 12058064]

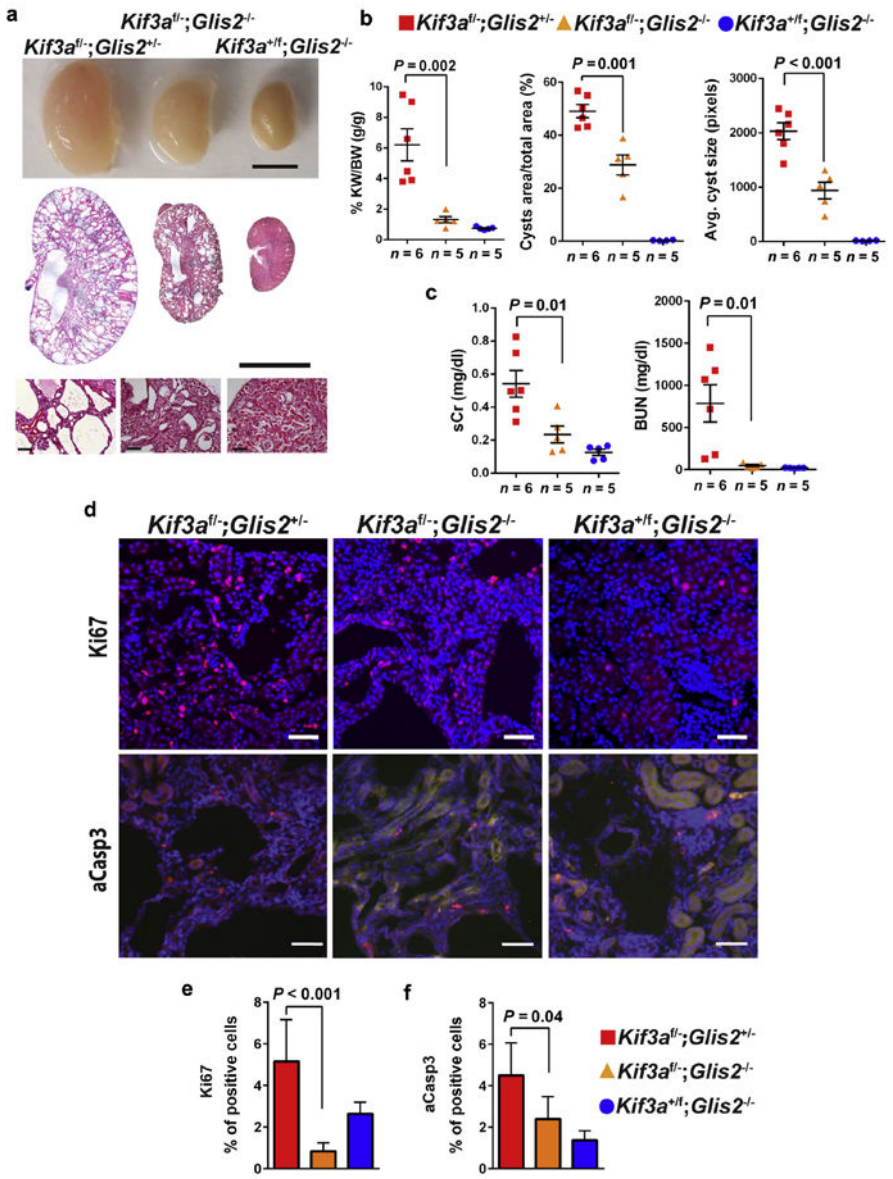

Figure 1. *Glis2* inactivation in *Kif3a*$^{f/-}$ knockouts results in reduced cyst growth, improved renal function, and decreased tubular cell proliferation and apoptosis

(**a**) Macroscopic representative images of *Kif3a*$^{f/-}$;*Glis2*$^{+/-}$, *Kif3a*$^{f/-}$;*Glis2*$^{-/-}$, and *Kif3a*$^{f/+}$;*Glis2*$^{-/-}$ mutant kidneys at P30 (upper panel) and the corresponding histology (hematoxylin and eosin staining) at low (middle panels) and high magnification (low panels). Kidneys of *Kif3a*$^{f/-}$;*Glis2*$^{-/-}$ double mutants are smaller, have fewer and smaller cysts, and have better preserved parenchyma when compared with *Kif3a*$^{f/-}$;*Glis2*$^{+/-}$ kidneys. Bars = 500 μm in the upper and middle panels and 100 μm in the lower panels. (**b**) Quantification of kidney weight to body weight ratio (KW/BW, g/g); cyst area (expressed as percentage of cyst area over total kidney area); and average cyst size in *Kif3a*$^{f/-}$;*Glis2*$^{+/-}$ (red squares), *Kif3a*$^{f/-}$;*Glis2*$^{-/-}$ (orange triangles), and *Kif3a*$^{f/+}$;*Glis2*$^{-/-}$ (blue circles). The number of mice in each experimental group is reported on the *x*-axis. Results are mean ± SD. *P* values were obtained by Student *t*-test. (**c**) Renal function indexes in *Kif3a*$^{f/-}$;*Glis2*$^{+/-}$,

Kif3a$^{f/-}$;*Glis2*$^{-/-}$, and *Kif3a*$^{+/f}$;*Glis2*$^{-/-}$ mice. Serum creatinine (sCr) and blood urea nitrogen (BUN) are expressed in mg/dl. The number of mice in each experimental group is reported on the *x*-axis. Results are mean ± SD. *P* values were obtained by Student *t*-test. (**d**) Representative immunofluorescence microscopy images of *Kif3a*$^{f/-}$;*Glis2*$^{-/-}$ double knockout kidneys compared with *Kif3a*$^{f/-}$;*Glis2*$^{+/-}$, *Kif3a*$^{+/f}$;*Glis2*$^{-/-}$ single mutants using antibodies to Ki67, a marker of proliferating cells, and activated caspase-3 (aCasp3), a marker of apoptosis. Bars = 100 μm. (**e**) Quantification of tubular proliferation in *Kif3a*$^{f/-}$;*Glis2*$^{+/-}$, *Kif3a*$^{f/-}$;*Glis2*$^{-/-}$, and *Kif3a*$^{+/f}$;*Glis2*$^{-/-}$ mice expressed as percentage of Ki67-positive cells over total number of cells (n = 3 mice per experimental group, 10 optical fields per mouse). Results are mean ± SEM. *P* values were obtained by Student *t*-test. (**f**) Quantification of the apoptotic tubular cells in *Kif3a*$^{f/-}$;*Glis2*$^{+/-}$, *Kif3a*$^{f/-}$;*Glis2*$^{-/-}$, and *Kif3a*$^{+/f}$;*Glis2*$^{-/-}$ mice obtained using the percentage of positive aCasp3 cells over total number of cells (n = 3 mice per experimental group, 10 optical fields per mouse). Results are mean ± SD. *P* values were obtained by Student *t*-test.

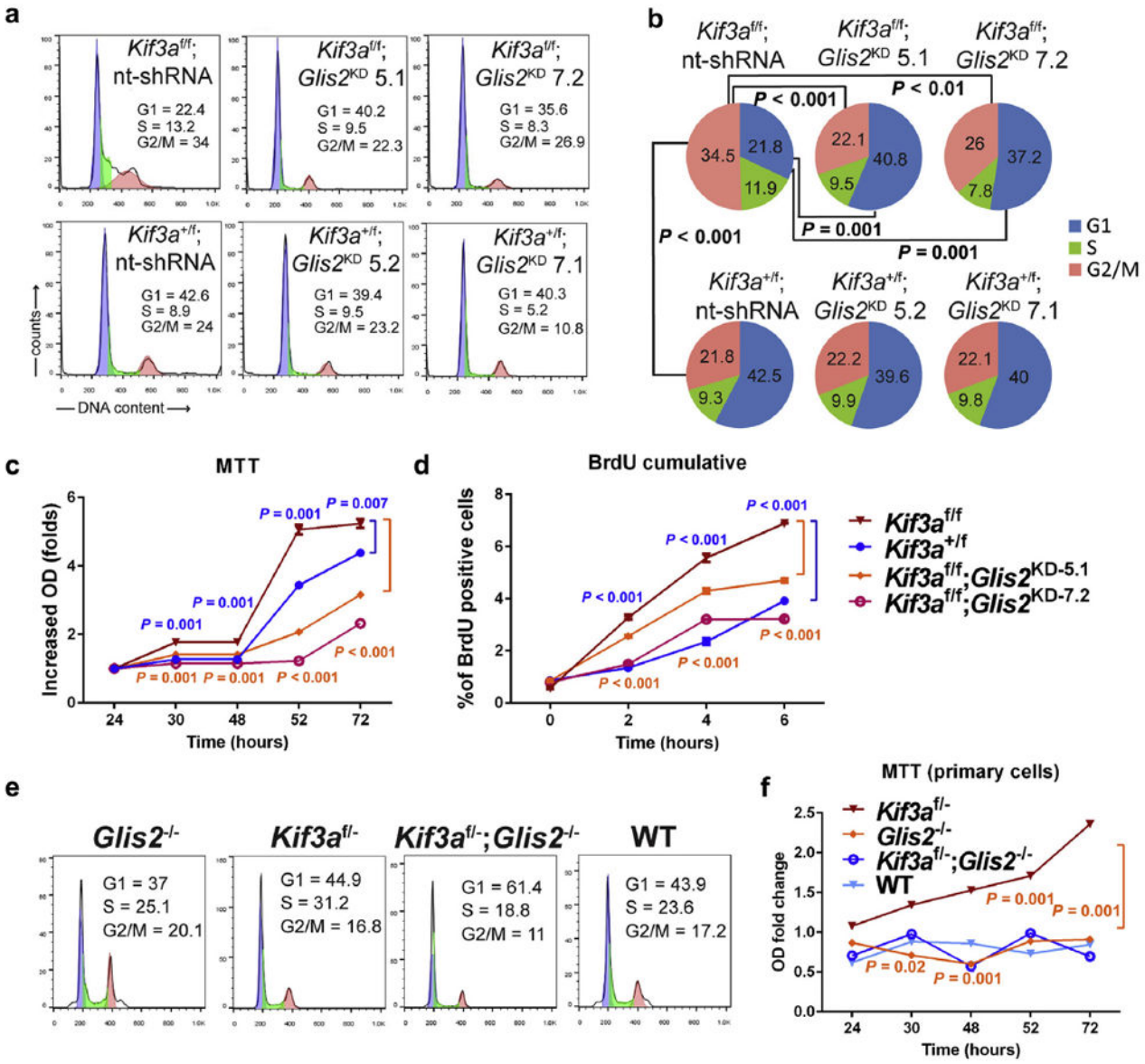

Figure 2. ***Kif3a*** **null kidney epithelial cells have accelerated cell cycle**

(**a**) Representative images of flow cytometry cell cycle analysis of *Kif3a*$^{f/f}$ and *Kif3a*$^{+/f}$ immortalized tubular cells stably transfected with nontargeting short hairpin RNA (nt-shRNA) or with *Glis2*-targeting shRNA (clones *Glis2*$^{KD\text{-}5.1}$ and *Glis2*$^{KD\text{-}7.2}$ for *Kif3a*$^{f/f}$ cells, *Glis2*$^{KD\text{-}5.2}$ and *Glis2*$^{KD\text{-}7.1}$ for *Kif3a*$^{+/f}$ cells; KDindicates knock-down).DNA content is represented on the *x*-axis; cell counts are shown on the *y*-axis. Counts of cellswith diploid (2n) DNA content (G1 phase) are highlighted in blue, tetraploid (4n) cells in pink (G2/M phase), and cells with intermediate DNA content (S phase) are highlighted in green. Insets report the relative cell cycle distribution (expressed as percentage) represented in each graphic. Percentages do not sumto 100%because debris and aggregated cells were excluded. (**b**) Quantification of the cell cycle distribution of *Kif3a*$^{f/f}$ and *Kif3a*$^{+/f}$ immortalized tubular cells with and without concomitant silencing of *Glis2*. Numbers in the pie chart correspond

to average percentage of cells in each phase of the cell cycle (n=4 independent experiments). Percentages do not sumto 100% because they were obtained after gating out debris and aggregated cells. Cells in G1 are represented in blue, cells S in green, and cells in G2/Min pink. *P* values were obtained by Student *t*-test. (**c**) Assessment by colorimetric assay (MTT) of doubling times of *Kif3a*$^{f/f}$ and *Kif3a*$^{+/f}$ immortalized tubular cells with andwithout concomitant silencing of *Glis2* at different time points. Values on the *y*-axis represent fold increase of optical density (OD). Doubling times are shorter in *Kif3a*$^{f/f}$ null cells than in the heterozygous control cells and decrease after shRNA-mediated *Glis2* silencing. n = 3 independent experiments. Results are mean ± SD. *P* values were obtained by Student *t*-test between *Kif3a*$^{f/f}$ and *Kif3a*$^{+/f}$ (blue brackets and values) and between *Kif3a*$^{f/f}$ and *Kif3a*$^{f/f}$;*Glis2*$^{KD\text{-}5.2}$ knockout–knock-down cells (orange bracket and values). (**d**) Cumulative BrdU incorporation in *Kif3a*$^{f/f}$ and *Kif3a*$^{+/f}$ immortalized tubular cells with and without concomitant *Glis2* silencing at different time points. Values on the *y*-axis represent the percentage of BrdU-positive cells at each time point. BrdU incorporation rates are increased in *Kif3a*$^{f/f}$ null cells compared with the heterozygous control cells and decrease after shRNA-mediated *Glis2* silencing. n = 3 independent experiments. Results are mean ± SD. *P* values were obtained by Student *t*-test between *Kif3a*$^{f/f}$ and *Kif3a*$^{+/f}$ (blue brackets and values) and between *Kif3a*$^{f/f}$ and *Kif3a*$^{f/f}$;*Glis2*$^{KD\text{-}5.2}$ knockout–knock-down cells (orange bracket and values). (**e**) Representative images of flow cytometry cell cycle analysis of primary tubular cells obtained from *Glis2*$^{-/-}$, *Kif3a*$^{f/-}$, *Kif3a*$^{f/-}$;*Glis2*$^{-/-}$ double knockouts, and wild-type mice as performed in (**a**). (**f**)MTT test onprimary tubular cells from *Kif3a*$^{f/-}$, *Glis2*$^{-/-}$, and *Kif3a*$^{f/-}$;*Glis2*$^{-/-}$ mice. Values on the *y*-axis represent fold increase of optical density, timepoints are on the *x*-axis. Doubling times are shorter in *Kif3a*$^{f/-}$ null cells than in *Glis2*$^{-/-}$ and *Kif3a*$^{f/-}$;*Glis2*$^{-/-}$ cells. Results are the average of 2 triplicate experiments and are mean ± SEM. *P* values were obtained by Student *t*-test.

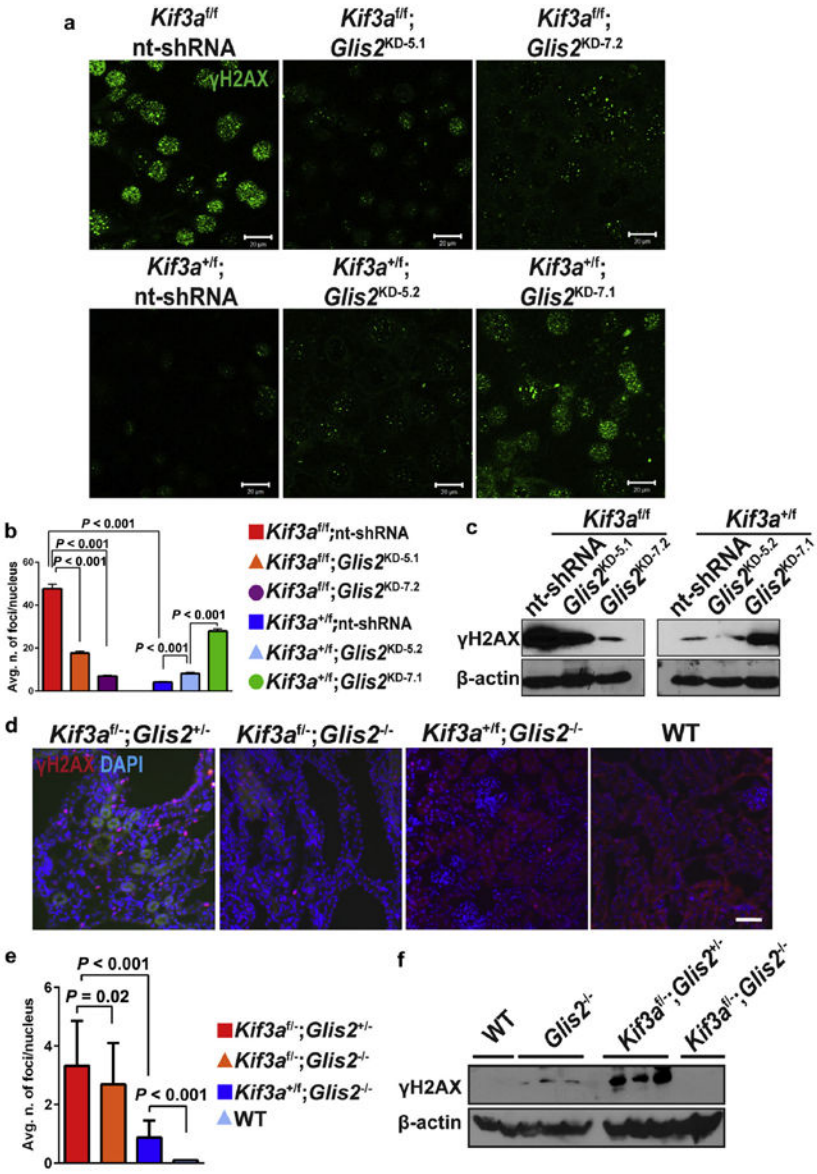

Figure 3. ***Kif3a*** **null kidney epithelial cells exhibit increased DNA damage and apoptosis**

(**a**) Representative immunofluorescence confocal microscopy images of antibody against phosphorylated histone 2AX (γH2AX) *in Kif3a*$^{f/f}$ and *Kif3a*$^{+/f}$ immortalized tubular cells with and without concomitant silencing of *Glis2*. (**b**) Quantification of DNA damage of (**a**). Values express average number of foci per nucleus (4 consecutive 3-μm confocal stacks from 10 consecutive images and 4 independent experiments). *Kif3a*$^{f/f}$ and *Glis2* knock-down *Kif3a*$^{+/f}$ heterozygous cells show increased DNA damage compared with the respective control cells. Short hairpin RNA (shRNA)-mediated *Glis2* silencing in *Kif3a*$^{f/f}$ cells results in reduction of the number of foci per nucleus. Results are mean ± SD. *P* values were obtained by Student *t*-test. (**c**) Western blots of *Kif3a*$^{f/f}$ and *Kif3a*$^{+/f}$ immortalized tubular cell lysates with and without concomitant silencing of *Glis2*, probed with an antibody against γH2AX. (**d**) Representative immunofluorescence microscopy images of sections of

Kif3a$^{f/-}$;*Glis2*$^{+/-}$, *Kif3a*$^{f/-}$;*Glis2*$^{-/-}$ double mutants, *Kif3a*$^{+/f}$;*Glis2*$^{-/-}$, and wild-type kidneys using an antibody against γH2AX and showing cells with DNA damage. (**e**) Quantification of (**d**). Values express percentage of positive cells (n = 3 mice, 10 consecutive optical fields per mouse). Results are mean ± SD. P values were obtained by Student t-test. (**f**) Western blot of wild-type (n = 2), *Glis2*$^{-/-}$ (n = 3), *Kif3a*$^{f/-}$;*Glis2*$^{+/-}$ (n = 3), and Kif3af$^{/+}$;*Glis2*$^{-/-}$ (n = 2) kidneys lysates probed with an antibody against γH2AX.

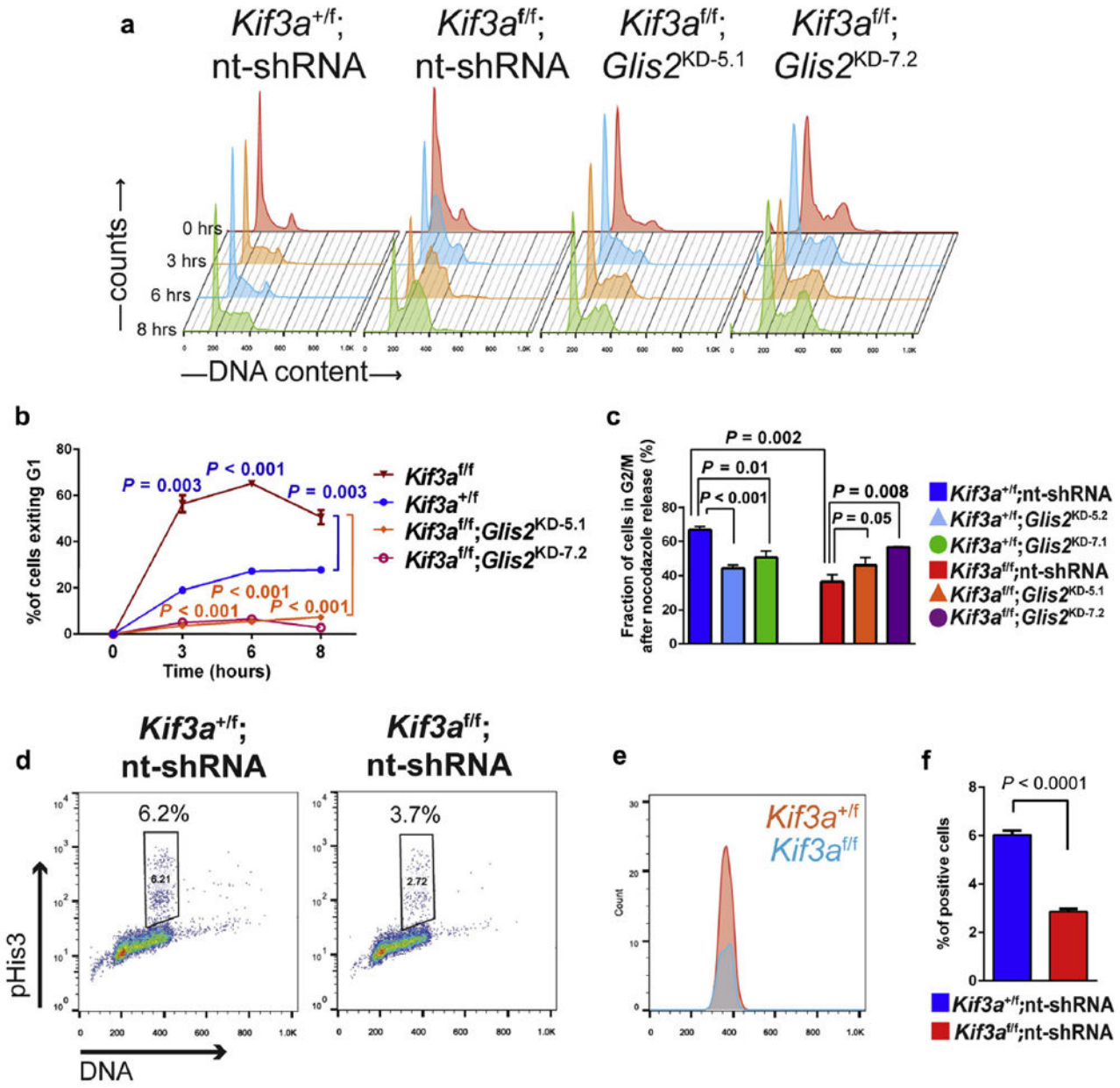

Figure 4. *Kif3a*$^{f/f}$ kidney epithelial cells have defective G1/S cell cycle checkpoint in the presence of DNA damage

(**a**) Representative flow cytometry cell cycle analysis of *Kif3a*$^{f/f}$ and *Kif3a*$^{+/f}$ immortalized tubular cells with and without concomitant silencing of *Glis2* after release of double thymidine block, which synchronizes cells in G1. DNA content is represented on the *x*-axis, cell counts on the *y*-axis. Samples were assayed at time 0 (in the presence of thymidine) and 3, 6, and 8 hours (after thymidine washout). (**b**) Quantification of (**a**). Values on the *y*-axis represent percentage of cells that exited G1 at each time point. $n = 3$ independent experiments. Results are mean ± SEM. *P* values were obtained by Student *t*-test between *Kif3a*$^{f/f}$ and *Kif3a*$^{+/f}$ (blue brackets and values) and between *Kif3a*$^{f/f}$ and *Kif3a*$^{f/f}$;*Glis2*$^{KD-5.1}$ knockout–knockdown cells (orange bracket and values). (**c**)

Quantification of *Kif3a*$^{f/f}$ and *Kif3a*$^{+/f}$ immortalized tubular cells with and without concomitant silencing of *Glis2*, after release of the nocodazole block ($n = 3$ independent samples). Values on the *y*-axis represent percentage of cells in G2/M, 6 hours after nocodazole washout. Results are mean ± SD. *P* values were obtained by Student *t*-test. (**d**) Flow cytometry bivariate analysis of *Kif3a*$^{f/f}$ and *Kif3a*$^{+/f}$ cells in mitosis, using an antibody against phosphorylated histone H3 (pHis3). Samples were enriched of mitotic cells by being exposed to nocodazole for 6 hours. Numbers are the percentage of pHis3-positive cells in G2/M. (**e**) Representative graphic of the same experiment, showing the cumulative distribution of *Kif3a*$^{f/f}$ compared with *Kif3a*$^{+/f}$ pHis3-positive cells. Cell counts are on the *y*-axis, fluorescence intensity is in the *x*-axis. (**f**) Graphic reporting the statistics of a triplicate experiment. Results are mean ± SD. *P* value was obtained by Student *t*-test. nt-shRNA, nontargeting short hairpin RNA.

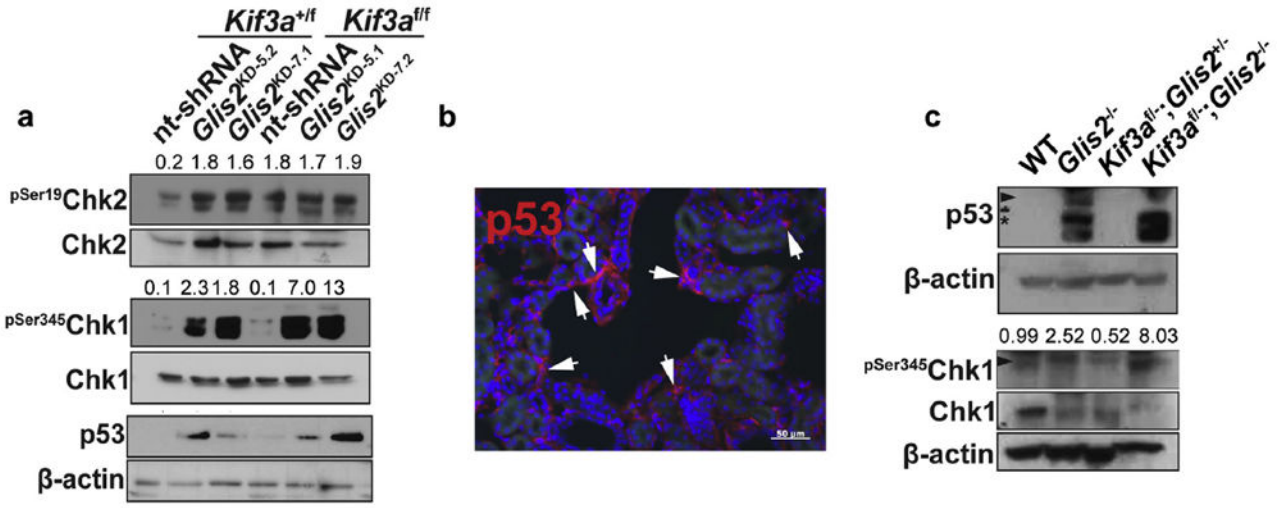

Figure 5. *Kif3a* and *Glis2* null kidney epithelial cells have defective and excessive activation of p53, respectively

(**a**) Western blot of *Kif3a*$^{+/f}$ and *Kif3a*$^{f/f}$ immortalized tubular cells with and without concomitant silencing of *Glis2* of total and Ser19 phosphorylated checkpoint kinase 2 (Chk2) (upper panels), total and Ser345 phosphorylated Chk1 (medium panels), and of p53 (lower panels). Chk2 is activated in *Kif3a*$^{f/f}$ cells compared with *Kif3a*$^{+/f}$ control cells independent of *Glis2* silencing. Chk1 is phosphorylated in the absence of *Glis2* in *Kif3a*$^{+/f}$ and *Kif3a*$^{f/f}$ cells. Stabilization of p53 is minimal in *Kif3a*$^{f/f}$ cells and is strongly induced by concomitant *Glis2* silencing. pSer19Chk2/Chk2 and pSer345Chk1/Chk1 densitometry ratios were calculated by digital analysis and are reported in correspondence of each lane. (**b**) Immunofluorescence microscopy image of *Kif3a*$^{f/-}$;*Glis2*$^{+/-}$ kidney probed with an antibody against p53 showing accumulation of p53 in numerous interstitial cells (white arrows). (**c**) Western blot of lysates of primary tubular cells obtained from wild-type, *Glis2*$^{-/-}$, *Kif3a*$^{f/-}$;*Glis2*$^{+/-}$, and *Kif3a*$^{f/-}$;*Glis2*$^{-/-}$ kidneys probed with an antibody against p53 (upper panels) and total and S345 phosphorylated Chk1 (lower panels). In the p53 Western blot, the dash corresponds to 50 knock-down (KD), the arrowhead indicates 53 KD, and the asterisk points to aspecific bands. The ratios of pSer345Chk1 (arrowhead) to Chk1 (lower panels) were calculated by digital analysis and are reported above each lane.

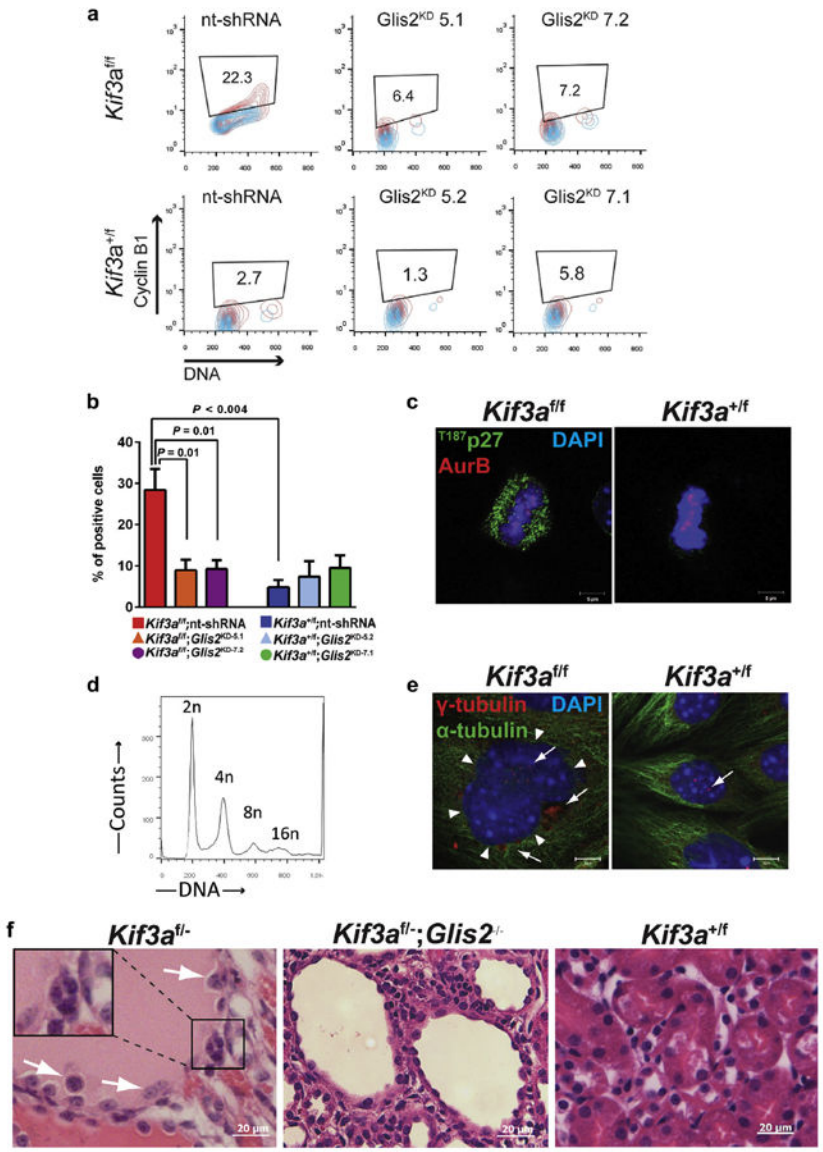

Figure 6. *Kif3* null kidney epithelial cells present ectopic accumulation of cyclin B1, premature mitosis, and centrosome amplification

(**a**) Flow cytometry of cyclin B1 in *Kif3a*$^{f/f}$ and *Kif3a*$^{+/f}$ immortalized tubular cells stably transfected with nontargeting short hairpin RNA (nt-shRNA) or with *Glis2*-targeting shRNA (clones *Glis2*$^{KD\text{-}5.1}$, *Glis2*$^{KD\text{-}7.2}$, *Glis2*$^{KD\text{-}5.2}$, and *Glis2*$^{KD\text{-}7.1}$; KD indicates knock-down), as performed in Figure 2a. Gates were established based on background fluorescence (nonimmune isotype antibody) for each sample. (**b**) Quantification of cyclin B1 content obtained from 4 independent replicates of the previous experiment. Values on the *y*-axis express percentage of positive cells for each cell group. Results are mean ± SEM. *P* values were obtained by Student *t*-test. (**c**) Immunofluorescence confocal microscopy images of *Kif3a*$^{f/f}$ and *Kif3a*$^{+/f}$ cells obtained with an antibody against phosphorylated threonine 87 of p27 (green channel) and the centromere marker Aurora kinase B. Condensed chromosomes with kinetocores (blue and red channels) indicate that the cells are in metaphase. Bars = 5

μm. (**d**) Flow cytometry cell cycle analysis of *Kif3af/f* immortalized tubular cells. Cell aggregates were not gated out for the analysis, to display polyploid cells with >4n DNA content. (**e**) Immunofluorescence microscopy images of *Kif3a*$^{f/f}$ and *Kif3a*$^{+/f}$ cells obtained with antibodies against the centrosomal marker γ–tubulin (red channel) and α-tubulin (green channel). DNA was stained with 4′,6-diamidino-2-phenylindole (DAPI) (blue channel). Arrows indicate fragmented (left panel) and normal centrosomes (right panel) in *Kif3a*$^{f/f}$ and *Kif3a*$^{+/f}$ cells. An abnormal megakaryon is also visible in the *Kif3a*$^{f/f}$ cell (delineated by the arrowheads). Bars = 5 μm. (**f**) Representative images of *Kif3a*$^{f/-}$, *Kif3a*$^{f/-}$;*Glis2*$^{-/-}$, and *Kif3a*$^{+/f}$ kidneys (hematoxylin and eosin). Arrows indicate tubular cells with megakarya or polyploidy. A polyploid cell is also highlighted at higher magnification in the inset (left panel). No nuclear abnormalities are apparent in *Kif3a*$^{f/-}$;*Glis2*$^{-/-}$, and *Kif3a*$^{+/f}$ kidneys. Bars = 20 μm.

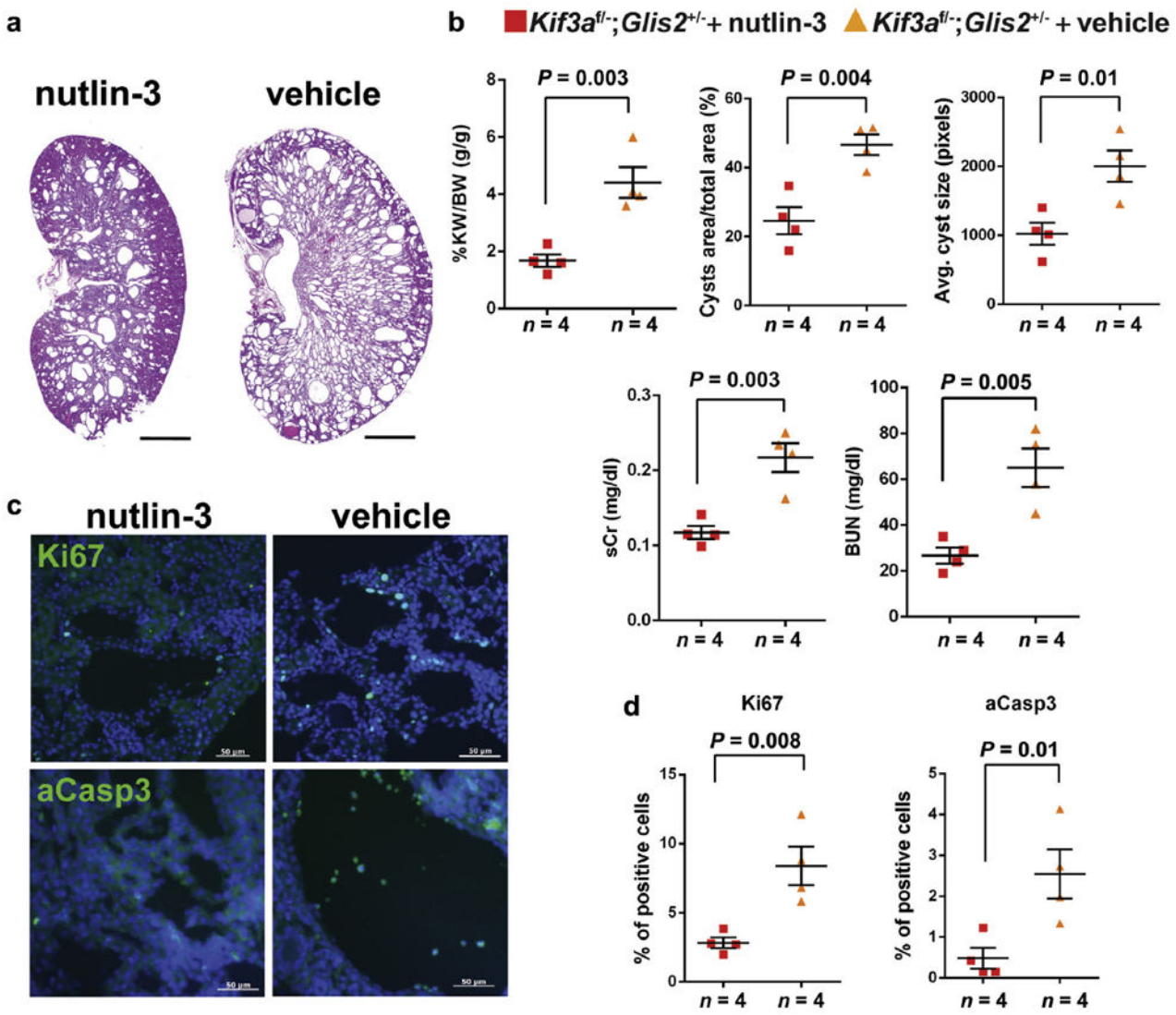

Figure 7. Pharmacological stabilization of p53 reduces cyst growth in *Kif3a*$^{f/-}$;*Glis2*$^{+/-}$ kidneys

(**a**) Kidneys of *Kif3a*$^{f/-}$;*Glis2*$^{+/-}$ treated with vehicle or with nutlin-3 for 10 days (hematoxylin and eosin). Kidneys of *Kif3a*$^{f/-}$;*Glis2*$^{+/-}$ nutlin-3-treated mice are smaller, have fewer and smaller cysts, and have better preserved parenchyma than vehicle-treated control kidneys. Bars = 1000 μm. (**b**) Quantification of kidney weight to body weight ratio (KW/BW, g/g), cyst area (expressed as percentage of cyst area over total kidney area), average cyst size, and renal function of *Kif3a*$^{f/-}$;*Glis2*$^{+/-}$ mice treated with vehicle or with nutlin-3. Serum creatinine (sCr) and blood urea nitrogen (BUN) are expressed in mg/dl. The number of mice in each experimental group is reported on the *x*-axis. Results correspond to mean ± SD. *P* values were obtained by Student *t*-test. (**c**) Representative immunofluorescence microscopy images of sections of *Kif3a*$^{f/-}$;*Glis2*$^{+/-}$ mice treated with vehicle or with nutlin-3, probed with an antibody against Ki67 and activated caspase 3 (aCasp3) to detect cycling and apoptotic cells, respectively. Bars = 50 μm. (**d**) Quantification of the previous experiment. The number of mice in each experimental group is reported on

the *x*-axis. Values express percentage of positive cells (10 consecutive optical fields per mouse). Results are mean ± SD. *P* values were obtained by Student *t*-test.

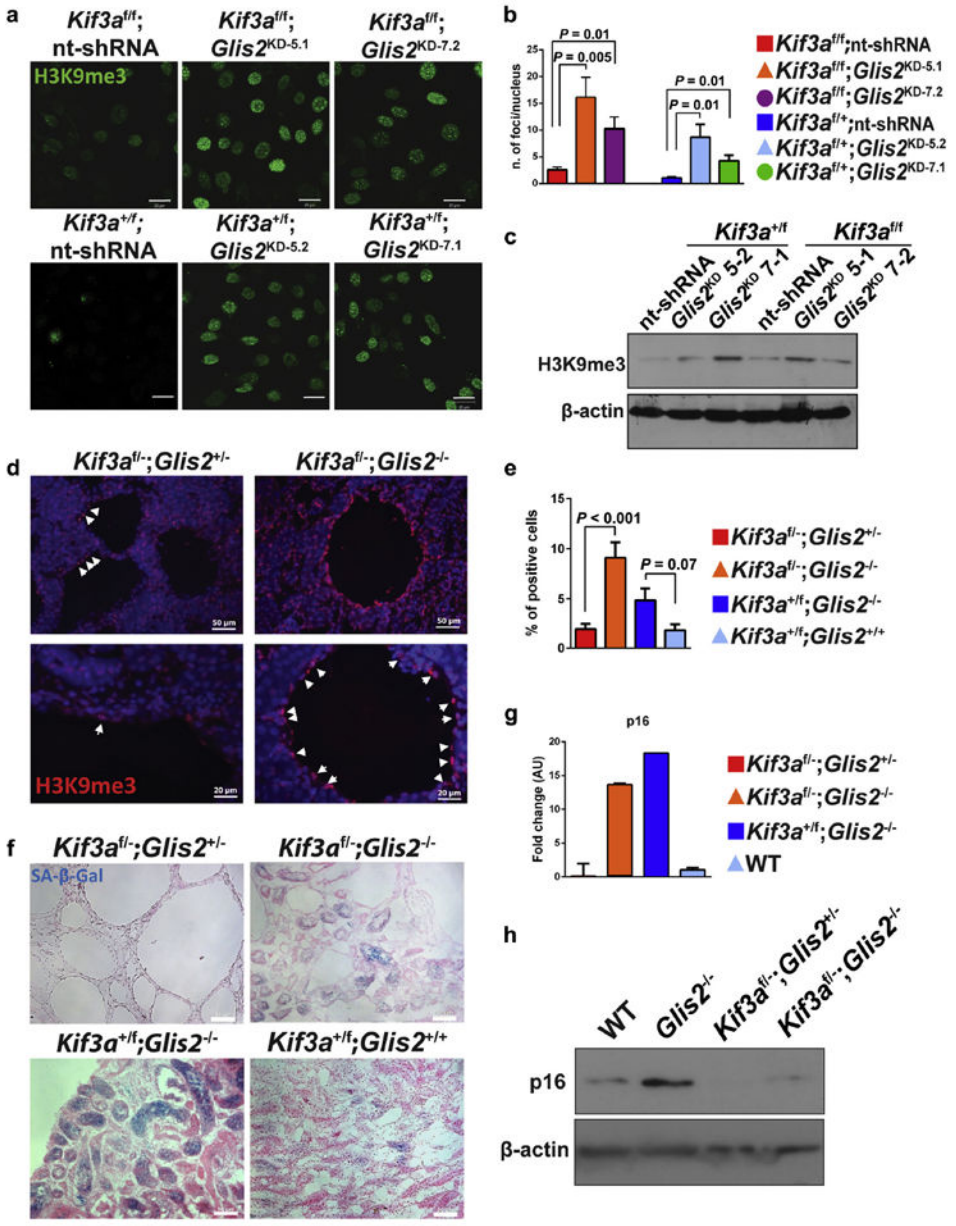

Figure 8. Loss of *Glis2* induces cellular senescence in kidney epithelial cells

(**a**) Representative immunofluorescence confocal microscopy images of *Kif3a*$^{f/f}$ and *Kif3a*$^{+/f}$ immortalized tubular cells with and without concomitant silencing of *Glis2*, obtained using an antibody against H3K9me3. Bars = 20 μm. (**b**) Quantification of the previous experiment, 3 independent samples per group (10 optical fields per sample, 4 stacks of 2 μm per field). Error bars are SD. *P* values were obtained by Student *t*-test. (**c**) Western blots of *Kif3a*$^{f/f}$ and *Kif3a*$^{+/f}$ immortalized tubular cells with and without concomitant silencing of *Glis2*, probed with an antibody against H3K9me3. H3K9me3 is increased in both cell lines after *Glis2* silencing. (**d**) Representative immunofluorescence microscopy images of kidney sections of *Kif3a*$^{f/-}$;*Glis2*$^{+/-}$, and *Kif3a*$^{f/-}$;*Glis2*$^{-/-}$ double mutant kidneys probed with an antibody against H3K9me3 at lower (upper panels, bars = 50 μm) and higher (lower panels, bars = 20

μm) magnification. (**e**) Quantification of H3K9me3 positive tubular cells *in vivo*. Ratio of positive cells was obtained dividing the number of positive nuclei by the total number of nuclei in 5 consecutive optical fields. $n = 3$ mice per group. Results are mean ± SEM. *P* values were obtained by Student *t*-test. (**f**) Bright field microscopy images of kidney sections of *Kif3a*$^{+/f}$;*Glis2*$^{+/+}$, *Kif3a*$^{f/-}$;*Glis2*$^{+/-}$, *Kif3a*$^{f/-}$;*Glis2*$^{-/-}$, and *Kif3a*$^{+/}$;*Glis2*$^{-/-}$ mice after 5-bromo-4-chloro-3-indolyl β-D-galactosidase (X-Gal) staining. Senescence-associated lysosomal β-galactosidase (SA-β-gal) activity (blue) was virtually absent in *Kif3a*$^{f/-}$;*Glis2*$^{+/-}$ kidneys but was clearly detected in *Kif3a*$^{f/-}$;*Glis2*$^{-/-}$ double mutants and more intensely in *Kif3a*$^{+/f}$;*Glis2*$^{-/-}$ kidneys. Bars = 50 μm. (**g**) Quantification by real-time polymerase chain reaction of p16 expression in primary tubular cells from *Kif3a*$^{f/-}$;*Glis2*$^{+/-}$, and *Kif3a*$^{f/-}$;*Glis2*$^{-/-}$, *Kif3a*$^{+/f}$;*Glis2*$^{-/-}$, and wild-type (WT) mice. Error bars are calculated from 3 experimental replicates and are SEM. (**h**) Western blot of lysates of primary tubular cells obtained from wild-type, *Glis2*$^{-/-}$, *Kif3a*$^{f/-}$;*Glis2*$^{+/-}$, and *Kif3a*$^{f/-}$;*Glis2*$^{-/-}$ kidneys, probed with an antibody against p16. The p16 protein levels are increased in *Kif3a*$^{f/-}$;*Glis2*$^{-/-}$ and *Glis2*$^{-/-}$, compared with *Kif3a*$^{f/-}$;*Glis2*$^{+/-}$ and wild-type cells, respectively.